

## Coincident Lake Drainage and Grounding Line Retreat at Engelhardt Subglacial Lake, West Antarctica

**Key Points:**

- Satellite altimetry detects second recorded drainage of Engelhardt Subglacial Lake in July 2021, triggered by an influx from an upstream lake
- The grounding line retreated by 2–13 km since the last drainage in 2003, linked to the retreat of Engelhardt Ice Ridge and ice plain ungrounding
- Satellite observations suggest that the 2021–24 lake drainage and grounding line retreat were largely independent processes

**Correspondence to:**

B. I. D. Freer,  
[bronyon.freer@gmail.com](mailto:bronyon.freer@gmail.com)


**Citation:**

Freer, B. I. D., Marsh, O. J., Fricker, H. A., Hogg, A. E., Siegfried, M. R., Floricioiu, D., et al. (2024). Coincident lake drainage and grounding line retreat at Engelhardt Subglacial Lake, West Antarctica. *Journal of Geophysical Research: Earth Surface*, 129, e2024JF007724. <https://doi.org/10.1029/2024JF007724>

Received 7 MAY 2024  
 Accepted 12 AUG 2024

**Author Contributions:**

**Conceptualization:** B. I. D. Freer, O. J. Marsh, H. A. Fricker, A. E. Hogg  
**Formal analysis:** B. I. D. Freer, H. A. Fricker, M. R. Siegfried  
**Investigation:** B. I. D. Freer, O. J. Marsh, H. A. Fricker, A. E. Hogg, M. R. Siegfried, D. Floricioiu  
**Methodology:** B. I. D. Freer, O. J. Marsh, H. A. Fricker  
**Project administration:** O. J. Marsh, A. E. Hogg  
**Resources:** B. I. D. Freer, M. R. Siegfried, D. Floricioiu, W. Sauthoff, R. Rigby, S. F. Wilson  
**Software:** B. I. D. Freer  
**Supervision:** O. J. Marsh, H. A. Fricker, A. E. Hogg  
**Validation:** B. I. D. Freer  
**Visualization:** B. I. D. Freer  
**Writing – original draft:** B. I. D. Freer

B. I. D. Freer<sup>1,2</sup> , O. J. Marsh<sup>1</sup> , H. A. Fricker<sup>3</sup> , A. E. Hogg<sup>2</sup> , M. R. Siegfried<sup>4</sup> ,  
 D. Floricioiu<sup>5</sup>, W. Sauthoff<sup>4</sup> , R. Rigby<sup>2</sup> , and S. F. Wilson<sup>2</sup> 

<sup>1</sup>British Antarctic Survey, Cambridge, UK, <sup>2</sup>School of Earth and Environment, University of Leeds, Leeds, UK, <sup>3</sup>Scripps Polar Center, Scripps Institute of Oceanography, UC San Diego, La Jolla, CA, USA, <sup>4</sup>Department of Geophysics, Colorado School of Mines, Golden, CO, USA, <sup>5</sup>DLR, German Aerospace Center, Oberpfaffenhofen, Germany

**Abstract** Antarctica has an active subglacial hydrological system, with interconnected subglacial lakes fed by subglacial meltwater. Subglacial hydrology can influence basal sliding, inject freshwater into the sub-ice-shelf cavity, and impact sediment transport and deposition which can affect the stability of grounding lines (GLs). We used satellite altimetry data from the ICESat, ICESat-2, and CryoSat-2 missions to document the second recorded drainage of Engelhardt Subglacial Lake (SLE), which began in July 2021 and discharged more than 2.3 km<sup>3</sup> of subglacial water into the Ross Ice Shelf cavity. We used differential synthetic aperture radar interferometry from RADARSAT-2 and TerraSAR-X alongside ICESat-2 repeat-track laser altimetry (RTL) and REMA digital elevation model strips to detect 2–13 km of GL retreat since the previous drainage event in 2003–06. Combining these satellite observations, we evaluated the mechanism triggering SLE drainage, the cause of the observed GL retreat, and the interplay between subglacial hydrology and GL dynamics. We find that: (a) SLE drainage was initiated by influx from a newly identified upstream lake; (b) the observed GL retreat is mainly driven by the continued retreat of Engelhardt Ice Ridge and long-term dynamic thinning that caused a grounded ice plain to reach flotation; and (c) SLE drainage and GL retreat were largely independent. We also discuss the possible origins and influence of a 27 km grounded promontory found to protrude seaward from the GL. Our observations demonstrate the importance of high-resolution satellite data for improving the process-based understanding of dynamic and complex regions around the Antarctic Ice Sheet margins.

**Plain Language Summary** Large volumes of water flow beneath the Antarctic Ice Sheet through an interconnected network of rivers and lakes. This water system impacts slipperiness at the base of the ice, affecting how fast it moves. It also delivers freshwater into the ocean, directly contributing to sea-level rise and increasing melt beneath the floating ice shelves. In this study, we use satellite data to track the 2021–24 drainage of Engelhardt Subglacial Lake in West Antarctica. This lake is located close to the Ross Ice Shelf grounding line, the point at the edge of the ice sheet where the ice first lifts off the bedrock and starts to float on the ocean. This region of the grounding line has retreated by up to 13 km since the last lake drainage in 2003–06. Here, we investigate what caused the drainage, the reasons for the grounding line retreat, and whether the two processes are connected. We also report the growth of a grounded promontory extending 27 km out to sea, which may be evidence of a former ice stream moraine or melt channel. These findings help to improve our limited understanding of the relationship between subglacial hydrology and grounding line dynamics in Antarctica.

### 1. Introduction

The Antarctic Ice Sheet (AIS) stores  $57.9 \pm 0.9$  m of sea-level rise equivalent (Morlighem et al., 2020) and is currently the largest source of uncertainty in future sea-level projections due to insufficient knowledge of ice sheet processes (IPCC, 2023; Seroussi et al., 2020). AIS dynamics are primarily controlled by the gravitational driving stress, conditions at the ice-bed interface (Paterson, 1994) and the “buttressing” effect of ice shelves (Gudmundsson et al., 2019). Subglacial hydrology can exert a strong influence on basal conditions and can accelerate basal melting, which might reduce ice shelf buttressing (Pelle et al., 2023); however, representations of subglacial hydrology are missing from most ice sheet and ice-ocean models (e.g., De Fleurian et al., 2018; S. Sun et al., 2020). This is largely due to the lack of direct observations of the Antarctic subglacial environment, which is difficult to access beneath multiple kilometers of ice (Priscu et al., 2021; Siegfried & Fricker, 2021; Siegfried et al., 2023).

© 2024. The Author(s).

This is an open access article under the terms of the [Creative Commons Attribution License](https://creativecommons.org/licenses/by/4.0/), which permits use, distribution and reproduction in any medium, provided the original work is properly cited.

Writing – review & editing:

B. I. D. Freer, O. J. Marsh, H. A. Fricker,  
A. E. Hogg, M. R. Siegfried, D. Floricioiu,  
W. Sauthoff, R. Rigby, S. F. Wilson

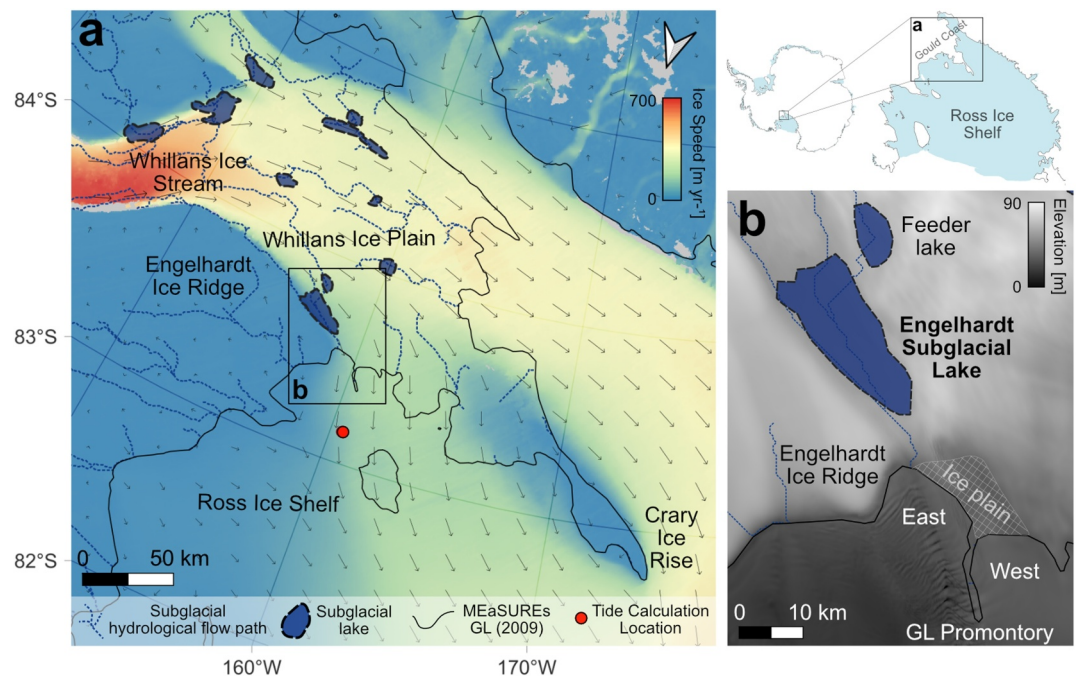


**Figure 1.** Location of Engelhardt Subglacial Lake (SLE) near the Ross Ice Shelf grounding line on the Gould Coast. (a) MEaSUREs ice velocity (Rignot et al., 2017) overlain with the location of known active subglacial lakes (Siegfried & Fricker, 2018), modeled hydrological pathways (Sauthoff & Freer, 2024) and the 2009 MEaSUREs GL (Rignot et al., 2016). (b) Zoom of SLE area in (a) showing the estimated subglacial lake boundary on the Reference Elevation Model of Antarctica (REMA) DEM mosaic (Howat et al., 2019). The locations of the east and west embayments and GL promontory are labeled alongside the estimated ice plain area (Brunt et al., 2010).

Active subglacial lakes are a key component of Antarctic subglacial hydrology; their fill-and-drain cycles have been shown to impact regional ice velocity (Scambos et al., 2011; Siegfried et al., 2016; Stearns et al., 2008), basal hydrology including bed slipperiness (Carter et al., 2013), nutrient fluxes (Hawkings et al., 2020), sediment transport (Carter et al., 2017; Drews et al., 2017; Siegfried et al., 2023; Simkins et al., 2017) and localized ice shelf melt rates (Marsh et al., 2016). Satellite altimetry provides a window into this behavior by measuring the signatures of surface uplift and subsidence associated with the respective filling and draining phases (Fricker et al., 2007, 2016; Malczyk et al., 2020; Neckel et al., 2021; Siegfried & Fricker, 2021). Despite recent advances in satellite observation capabilities, we still do not understand many of the processes related to active subglacial lakes (e.g., Stubblefield et al., 2023) and they remain under-sampled in space and time (Siegfried & Fricker, 2021). Key questions remain regarding the triggers and mechanisms of subglacial lake drainage (Siegfried et al., 2023), the timescales for fill-and-drain cycles, and the influence of drainage on grounding zone (GZ) dynamics (Carter et al., 2017; Simkins et al., 2017).

In this study, we present the first observations of the 2021–24 drainage of Engelhardt Subglacial Lake (SLE) in West Antarctica using high resolution satellite measurements from Ice, Cloud and land Elevation Satellite-2 (ICESat-2). This event is only the second drainage on record at this lake and provides a rare opportunity to investigate the co-evolution of an actively draining subglacial lake and the downstream grounding line (GL). Leveraging improvements in spatial and temporal sampling of satellite instruments over the past two decades, we compile a 21-year satellite record of ice-sheet surface elevation change associated with the fill-and-drain cycle of SLE, examine the GL evolution before and during the 2021–24 drainage event, and evaluate the interactions between these processes.

## 2. Study Region

Engelhardt Subglacial Lake (SLE) is one in a network of active subglacial lakes beneath Whillans Ice Plain on the Gould Coast, first discovered in the mid-2000s (Fricker et al., 2007). SLE occupies a ~250–350 km<sup>2</sup> region fed by water originating from the upper Kamb and Whillans ice streams (Figure 1a; Carter et al., 2013). Between

October 2003 and June 2006, ICESat laser altimetry detected a  $\sim 9$  m drop in surface elevation at SLE, which was interpreted as a signal of drainage (Fricker et al., 2007). This was the first evidence of SLE drainage in the satellite record, discharging  $\sim 2.0$  km<sup>3</sup> subglacial water across the Ross Ice Shelf (RIS) GL  $\sim 10$  km downstream. SLE slowly refilled over the next 15 years (Siegfried & Fricker, 2018).

SLE is one of the only active subglacial lakes in Antarctica located within 10 km of the GL (Siegfried & Fricker, 2018). The GL downstream of SLE comprises an east and west embayment separated by a grounded promontory (Figure 1b). In the east embayment, the GL has been retreating by 300–500 m yr<sup>-1</sup> since at least 1963, with the most rapid retreat focused on the GL along Engelhardt Ice Ridge, formerly called Ridge B/C (Bind-schadler & Vornberger, 1998; Fricker et al., 2007). It was suggested that the 2003–06 SLE drainage could be linked to the observed GL retreat here, but it remains an open question whether the GL retreat triggered the lake drainage or whether the drainage led to the GL retreat (Fricker & Scambos, 2009). In the west embayment, there is greater uncertainty in the GL position, with a small ice plain identified just inland extending to the break-in-slope (Figure 1b; Brunt et al., 2010; Horgan & Anandakrishnan, 2006). ICESat and RADARSAT-2 measurements indicate that this ice plain was grounded until at least 2009 (Brunt et al., 2010; Rignot et al., 2016), and so was likely unaffected by the 2003–06 SLE drainage.

### 3. Data and Methods

#### 3.1. Satellite Data

*Satellite laser altimetry:* NASA's ICESat laser altimetry mission operated between February 2003 and October 2009, and carried a 1,064 nm laser altimeter that provided high precision ( $<0.1$  m) repeat surface elevation retrievals every  $\sim 170$  m along-track (Schutz et al., 2005). We used the GLAH06 Level-1B Global Elevation (version 34) product (Zwally et al., 2014) with surface elevations relative to the WGS84 ellipsoid corrected for tides, atmospheric delays, surface characteristics, Gaussian-Centroid offset (Borsa et al., 2014) and saturation (X. Sun et al., 2017).

ICESat-2 was launched in 2018. Its photon-counting 532 nm laser altimeter estimates surface elevation along its 1387 reference ground tracks (RGTs), each comprising six beams and repeating every 91 days (Magruder et al., 2021). We used data from: (a) the Level 3A Land Ice Height data product (ATL06 version 6; Smith et al., 2023) from cycles 3–23 (April 2019–April 2024), which provides mean surface elevation averaged along 40 m ground track (GT) segments spaced 20 m apart; and (b) the Level 3B Gridded Antarctic Land Ice Height Change product (ATL15 version 4; Smith et al., 2024), which provides 1 km gridded elevation change data, currently available at a quarter-year time step between April 2019 and January 2024 (note the ATL15 coverage period is 3 months shorter than for ATL06).

*Satellite radar altimetry:* The European Space Agency's CryoSat-2 mission launched in 2010, carrying a synthetic aperture interferometric (SARIn) radar altimeter. Its SARIn mode provides elevation retrievals every 300 m along-track with an effective spatial resolution of 380–410 m along-track and  $\sim 1.7$  km across-track (McMillan et al., 2013). We used CryoSat-2 SARIn data over SLE between 2010 and 2020, which we swath-processed at 250 m spatial resolution and averaged at 3-monthly intervals using a linear fit method (after McMillan et al., 2014; Shepherd et al., 2019; Slater et al., 2021).

*Synthetic aperture radar (SAR):* RADARSAT-2 and TerraSAR-X are side-looking SAR instruments with left-looking capabilities (required to cover the high southern latitudes), launched in 2007. We generated double-difference interferograms (DInSAR) over the SLE region and its GL using RADARSAT-2 data from 2009 and TerraSAR-X data from 2012, 2016 and 2023. Multilooked imagery for both satellites was georeferenced to Bedmap2 surface elevations (Fretwell et al., 2013). Image dates, processing information and sampled tides are provided in Table 1.

*Optical imagery:* We used the REMA digital elevation model (DEM) mosaic (version 2) and strip (version 4.1) data sets created with sub-meter resolution Maxar optical satellite imagery (Howat et al., 2019). The strip DEMs are time-stamped to allow for change detection analysis, but are not registered vertically to satellite altimetry.

**Table 1**

*Image Processing Information and Acquisition Time for All RADARSAT-2 and TerraSAR-X DInSAR Scenes Used in This Study*

DInSAR date and Satellite	Spatial resolution [m] (ground range × azimuth)	DEM for geocoding	Pass date/Time	Tide height, corrected IBE [m]	Expected height difference [m] $[t2 - t1] + [t2 - t3]$
February 2009 RADARSAT-2	$12 \times 5$ ( $2 \times 6$ multilooking)	Bedmap2 (50 m grid)	t1 2009-02-19 14:31:00	+0.337	−1.79
			t2 2009-03-15 14:31:00	−0.811	
			t3 2009-04-08 14:31:00	−0.171	
September 2012 TerraSAR-X	$2.5 \times 3.3$ ( $4 \times 4$ multilooking)	Bedmap2 (8 m grid)	t1 2012-09-02 14:38:00	−0.349	−0.872
			t2 2012-09-13 14:38:00	−0.507	
			t3 2012-09-24 14:38:00	+0.206	
April 2016 TerraSAR-X	$2.5 \times 3.3$ ( $4 \times 4$ multilooking)	Bedmap2 (8 m grid)	t1 2016-04-08 14:47:00	−0.460	+0.679
			t2 2016-04-19 14:47:00	−0.076	
			t3 2016-04-30 14:47:00	−0.372	
July 2023 TerraSAR-X	$2.5 \times 3.3$ ( $4 \times 4$ multilooking)	Bedmap2 (8 m grid)	t1 2023-06-27 06:31:00	−0.259	+0.166
			t2 2023-07-08 06:31:00	+0.023	
			t3 2023-07-19 06:31:00	+0.139	
October 2023 TerraSAR-X	$2.5 \times 3.3$ ( $4 \times 4$ multilooking)	Bedmap2 (8 m grid)	t1 2023-10-03 06:48:00	−0.608	+0.691
			t2 2023-10-14 06:48:00	−0.359	
			t3 2023-10-25 06:48:00	−0.802	

*Note.* The tidal heights for each individual pass were calculated at the location shown in Figure 1 [83.161°S, 160.5°W] using the CATS2008 model (Howard et al., 2019), corrected for the inverse barometer effect (IBE) using the daily air pressure values from the National Center for Environmental Prediction and the National Center for Atmospheric Research Reanalysis (NCEP/NCA). The expected vertical height difference for each DInSAR is calculated using the tides from individual passes:  $[t2 - t1] + [t3 - t2]$ .

## 3.2. Methods

### 3.2.1. Surface Elevation Change

We generated a time-series of surface elevation change associated with the fill-and-drain cycle of SLE by combining elevation estimates from three satellite altimeter missions (Figure 2). We selected three  $\sim 3$  km<sup>2</sup> crossover zones (CZs) at locations over the lake with the highest density of intersecting ICESat and ICESat-2 RGTs. A fourth CZ slightly upstream of the lake contained only ICESat-2 tracks. For each section of the ICESat/ICESat-2 track intersecting a CZ, we calculated the mean along-track elevation per repeat cycle from the GLAH06 and ATL06 data sets, providing 3 time-series of elevation change at CZ1–3 from 2003–09 (ICESat) and 2019–24 (ICESat-2), and a time-series at CZ4 for 2019–24 (ICESat-2 only). To extend the record from 2010 to 2020 we calculated a time-series of mean elevation within each CZ from the swath-processed CryoSat-2 data. We used the ICESat-2 ATL15 gridded elevation data set to determine the spatial extent of drainage and the total ice and (inferred) water volume displacement at quarter-year intervals from 2019–24 (note this does not cover the entire duration of drainage).



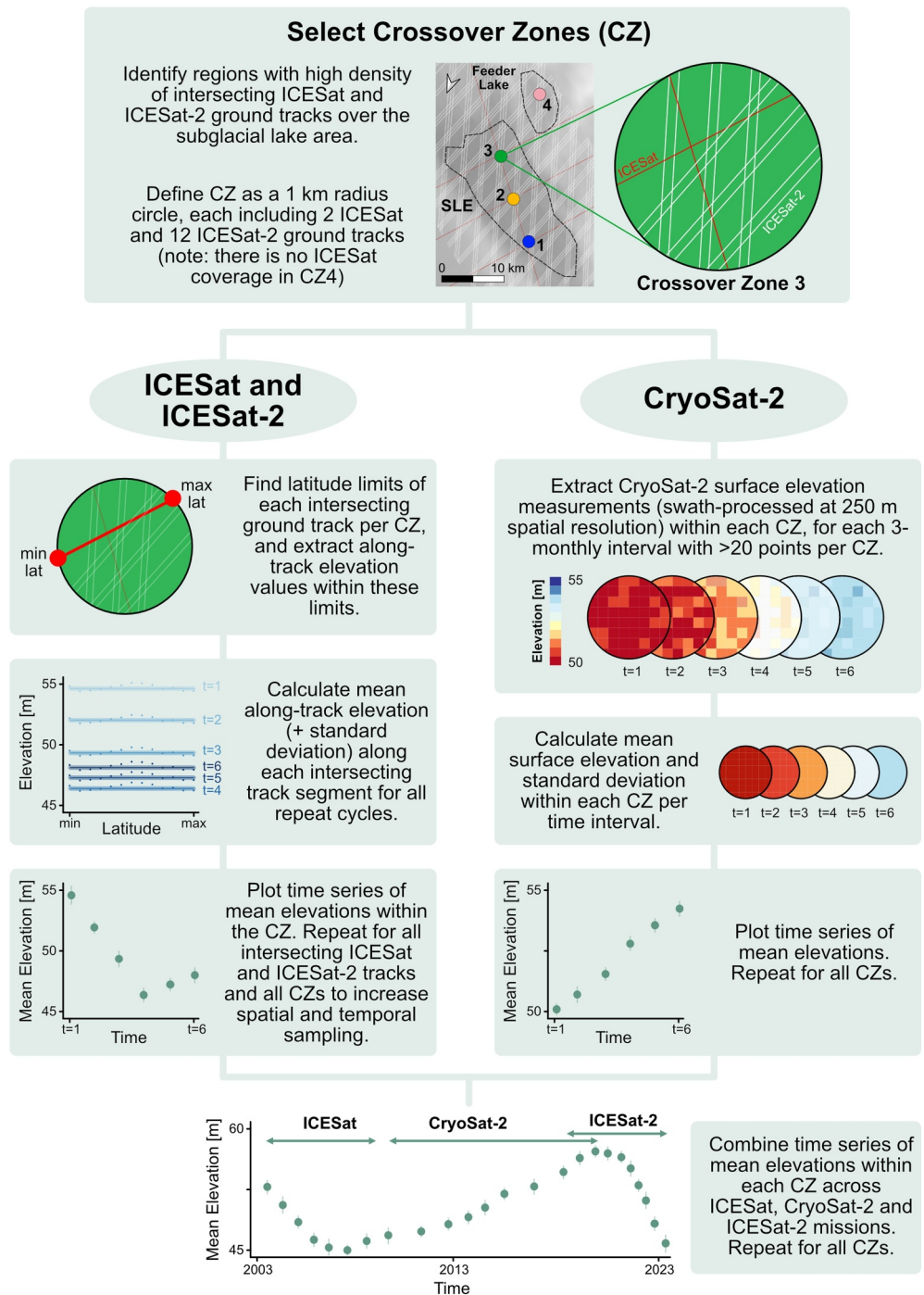


**Figure 2.** Combining satellite laser and radar altimetry elevations. Flowchart of methods used to derive a time-series of mean ice sheet surface elevation values within each crossover zone (CZ1–4) at SLE using elevation data from ICESat (2003–09) and ICESat-2 (2019–24) laser altimetry and CryoSat-2 radar altimetry (2010–20). Note that all elevation values are illustrative.

### 3.2.2. Subglacial Hydrological Flow Pathways

We used static grids of ice surface elevation from the REMA mosaic (Howat et al., 2019) and ice thickness (from which bed elevation can be inferred; Morlighem et al., 2020) to predict the subglacial water flow routing pathways beneath Whillans Ice Plain based on hydropotential gradients. Hydropotential gradients control where water is

driven to flow by gravitational potential (bed elevation) and ice overburden pressure (Shreve, 1972), given by Equation 1:

$$\nabla\varphi = \rho \cdot g \cdot \nabla z \cdot \nabla P_w \quad (1)$$

where  $\nabla\varphi$  is the hydropotential gradient,  $\rho$  is the density of water,  $g$  is gravitational acceleration,  $z$  is bed elevation, and  $P_w$  is water pressure. Flow routing pathways were modeled based on the hydropotential surface using the Python package `pysheds` (Bartos, 2020).

### 3.2.3. Grounding Line Change

We located the GL with two independent methods: (a) DInSAR: we traced the landward boundary of the dense fringe belt associated with the vertical tidal motion of the ice (the inland limit of tidal flexure, typically described as Point F; Rignot et al., 2011) in each RADARSAT-2 and TerraSAR-X double-difference interferogram (Marsh et al., 2024; dates in Table 1); (b) ICESat-2: we used a repeat track laser altimetry (RTLA) methodology, described in Freer et al. (2023), to provide GL locations at higher temporal sampling (intra-annual) from 2019–24. This method takes repeat ATL06 elevations along a single ICESat-2 RGT for each repeat cycle and compares them to a reference profile taken at the lowest sampled tide to calculate elevation anomalies. From this we obtained the inland limit of tidal flexure (Point F) per repeat cycle, which is the same GL proxy as detected by DInSAR. We repeated this for all RGTs crossing the GL.

### 3.2.4. Engelhardt Ice Ridge Retreat

We assessed the retreat of Engelhardt Ice Ridge along ICESat RGT 172 and ICESat-2 RGT 343 ground track 1R (GT1R) that cross the northern face of the ridge. We extended both time-series between the ICESat and ICESat-2 periods by sampling elevations along each track from all available REMA DEM strips 2012–22. Where there were small geolocation errors, we manually adjusted the elevation profiles (by up to  $\pm 6$  m) based on the top ridge surface. We calculated ridge retreat rates across the time-series at the 40-m elevation contour.

## 4. Results

### 4.1. Surface Elevation Change at SLE

Combined satellite altimetry data sets from the ICESat, ICESat-2 and CryoSat-2 missions yielded a 21-year time-series of surface elevation showing the activity of SLE (Figure 3c). This captured drainage in 2003–06 (Fricker et al., 2007), the 15-year refilling period (Siegfried & Fricker, 2018), and the onset of a second drainage event in July 2021.

Between September 2020 and the onset of SLE drainage in July 2021, we observed a  $\sim 3$  m drop in surface elevations in a small region upstream of SLE (CZ4 in Figure 3c) as surface elevations over SLE continued to rise at a slightly faster rate. Considering its location on the modeled upstream hydrologic flow path (Figure 1b) and its correlation to SLE drainage, we interpret this as a signal from a newly identified upstream “feeder lake” draining directly into SLE. This upstream lake was not well-sampled by ICESat due to its sparser track spacing (Figure 3a); however, ICESat-2 has denser sampling and the repeat-track surface elevation profiles along RGT 343 GT1R show a sharp fill-and-drain event here immediately preceding SLE drainage (Figures 3 and 4).

Between July 2021 and January 2024, surface elevations over the SLE area fell by a median value of 10.8 m (interquartile range (IQR):  $-13.7$  to  $-6.7$  m; as calculated from ICESat-2 ATL15; Figure 4), and by more than 15 m in the central lake area (Figures 3b and 3c). The rate of surface-lowering accelerated to reach a maximum in July 2023 (Figure 4t), after which it began to decrease, at first from the upstream end (Figures 4q–4t). SAR backscatter images show the development of surface crevasses along the margin of the lake caused by this drainage-induced subsidence (Figure 5a). Based on the subsidence area and total elevation decrease, we estimate that the lake drained at least  $2.3 \text{ km}^3$  of subglacial water into the RIS cavity between July 2021 and January 2024. This calculation assumes that total displaced ice volume equals the displaced water volume, which we acknowledge may not always hold due to the effects of viscous ice flow (Sergienko et al., 2007; Stubblefield et al., 2021, 2023). The extended ICESat-2 ATL06 elevation record shows surface subsidence in the downstream

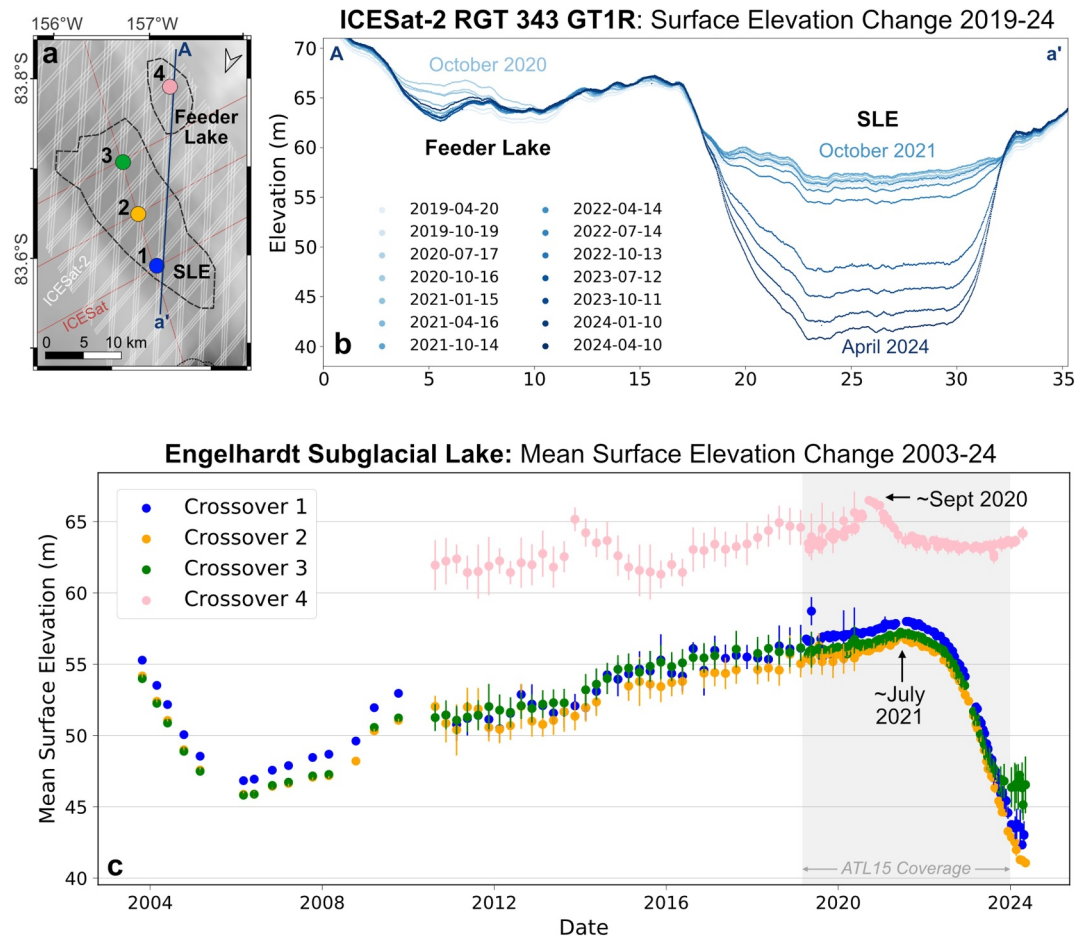


**Figure 3.** Satellite laser and radar altimetry measurements of surface elevation change at SLE, 2003–24. (a) Location of the four crossover zones (CZ1–4) used to calculate mean elevation change at SLE, and ICESat (red) and ICESat-2 (white) RGTs. (b) Repeat surface elevation profiles along ICESat-2 RGT 343 ground track 1R (GT1R), April 2019–April 2024; location in (a). (c) 21-year time-series of mean surface elevation at SLE, measured within CZ1–4 by ICESat (2003–09), CryoSat-2 (2010–20) and ICESat-2 (2019–24). Error bars represent one standard deviation of along-track surface elevation measurements within each CZ (note error bars are too small to be visible for some ICESat and ICESat-2 data points). Gray shading shows the ICESat-2 ATL15 coverage period (used in Figure 4).

part of the SLE continued until at least April 2024 (likely continuing for a couple of months beyond this), leading to a total estimated drainage period of 34–36 months.

## 4.2. Grounding Line Retreat

The SAR, laser altimetry and DEM data revealed extensive GL reconfiguration and surface elevation change across the entire region downstream of SLE between 2009 and 2023. The observed retreat exhibits spatial diversity, with GL retreat and ice thinning observed in the east and west embayments alongside GL advance and ice thickening along the central GL promontory (Figure 6). We describe these regional patterns separately.

### 4.2.1. East Embayment

In the east embayment, comparison of the DInSAR data revealed that there was 2–3 km of GL retreat between 2009 and 2023 (Figure 6b). By 2023, at its most landward position the GL was just ~7 km from SLE. The GL retreat was predominantly focused along Engelhardt Ice Ridge, which coincides with the ongoing longer-term retreat of the steep slope upstream of the GL (Figure 7; Bindshadler & Vornberger, 1998; Fricker & Scambos, 2009; Fricker et al., 2007). SAR repeat sampling here is infrequent; however, using the higher frequency sampling from ICESat, ICESat-2, and REMA we were able to estimate the mean *rate* of retreat of the ridge in

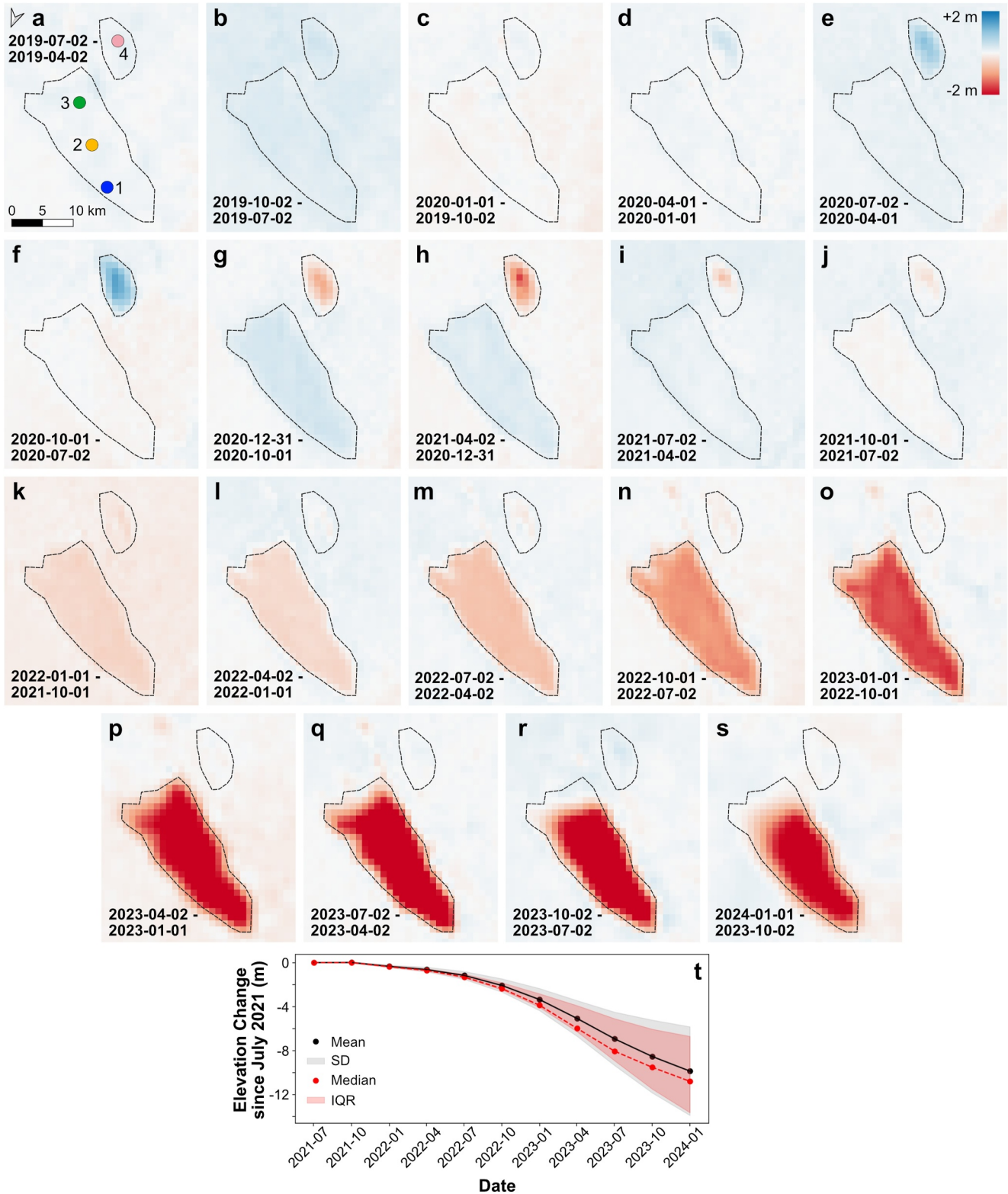


**Figure 4.** Temporal evolution of surface elevation change at SLE, April 2019–January 2024. (a–s) ATL15 gridded surface elevation change at SLE and its upstream feeder lake between consecutive quarter-year intervals (Smith et al., 2024). Lake boundaries (dashed black lines) were manually delineated based on the observed surface subsidence area, and circles in (a) mark the location of crossover zones 1–4. (t) Mean and median cumulative elevation change within the SLE boundary from the onset of SLE drainage (July 2021–January 2024). Black and red shaded areas show the standard deviation (SD) and inter-quartile range (IQR).



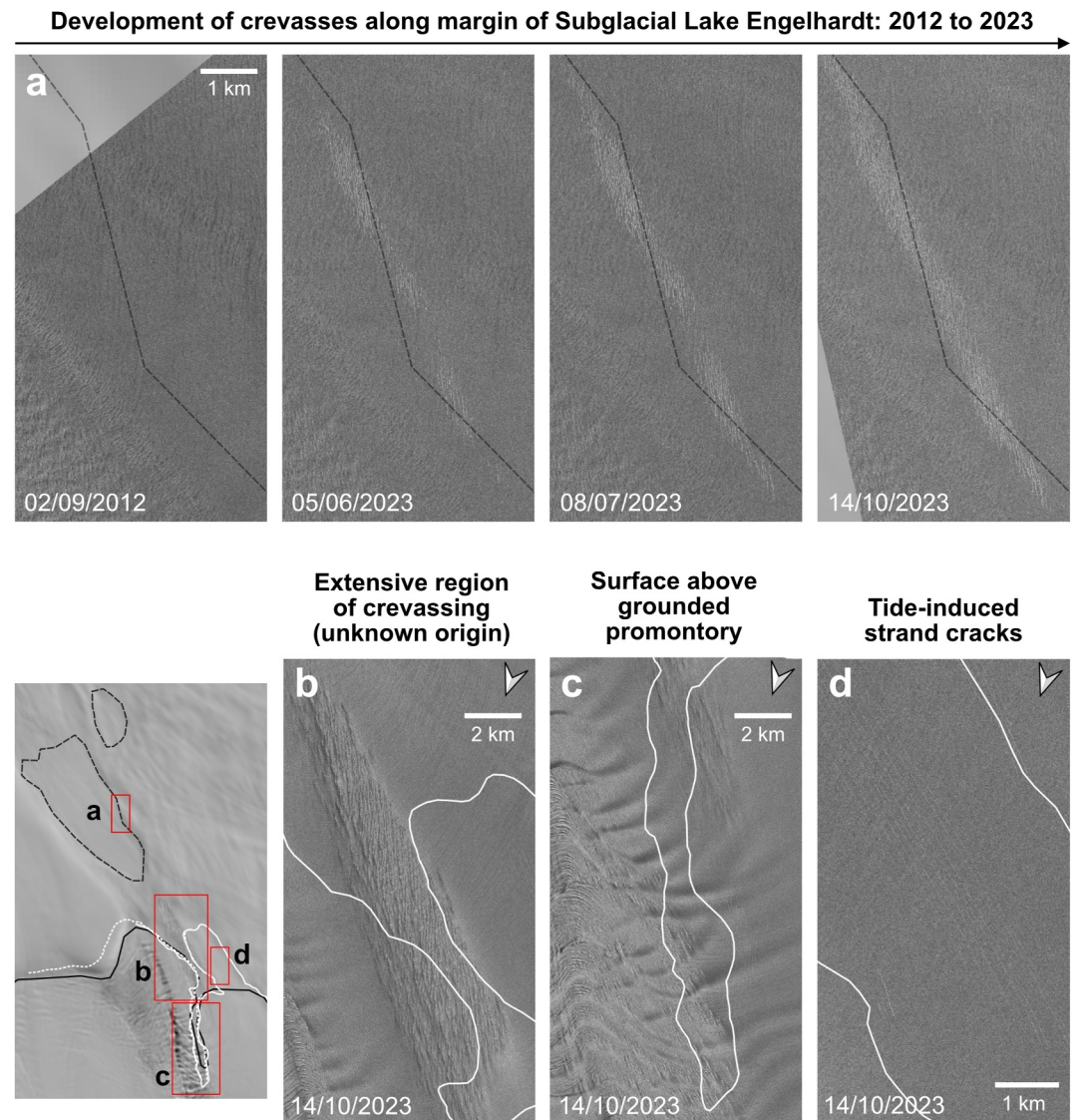


**Figure 5.** SAR imagery showing surface damage and crevassing at SLE and the GZ. (a) Time-series of TerraSAR-X multi-look backscatter images 2012–23 along the SW margin of SLE, showing the development of crevasses caused by drainage-induced surface subsidence (cf. Fried et al., 2014). (c) Extensive region of crevassing downstream of SLE and at the upstream end of the GZ promontory. (d) Large surface undulations and more complex surface crevassing around the GZ promontory. (e) Tide-induced strand cracks parallel to the newly retreated GL of the west embayment.

between the available DInSAR images, by tracking the migration of the 40-m elevation contour along two intersecting ground tracks (Figures 7e and 7f). This showed that the ridge retreated at a constant rate of 0.1–0.2 km yr<sup>-1</sup> between 2003 and 2024. Notably, there was no acceleration or deceleration in ridge retreat following the onset of SLE drainage until a slight acceleration was observed in 2024 (Figure 7f). The ridge retreat manifested in a strong (>10 m) thinning signal observed in the ICESat-2 record along this section of the GL between 2019 and 2024 (Figure 6d).

#### 4.2.2. West Embayment

In the west embayment, the GL retreated by ~13 km between 2009 and 2023 into a region previously identified as a grounded ice plain (Figures 6a and 6b; Brunt et al., 2010). We used the SAR and ICESat-2 data to investigate the timing of this ungrounding as well as the thinning rate and tidal flexure of the ungrounded ice plain.

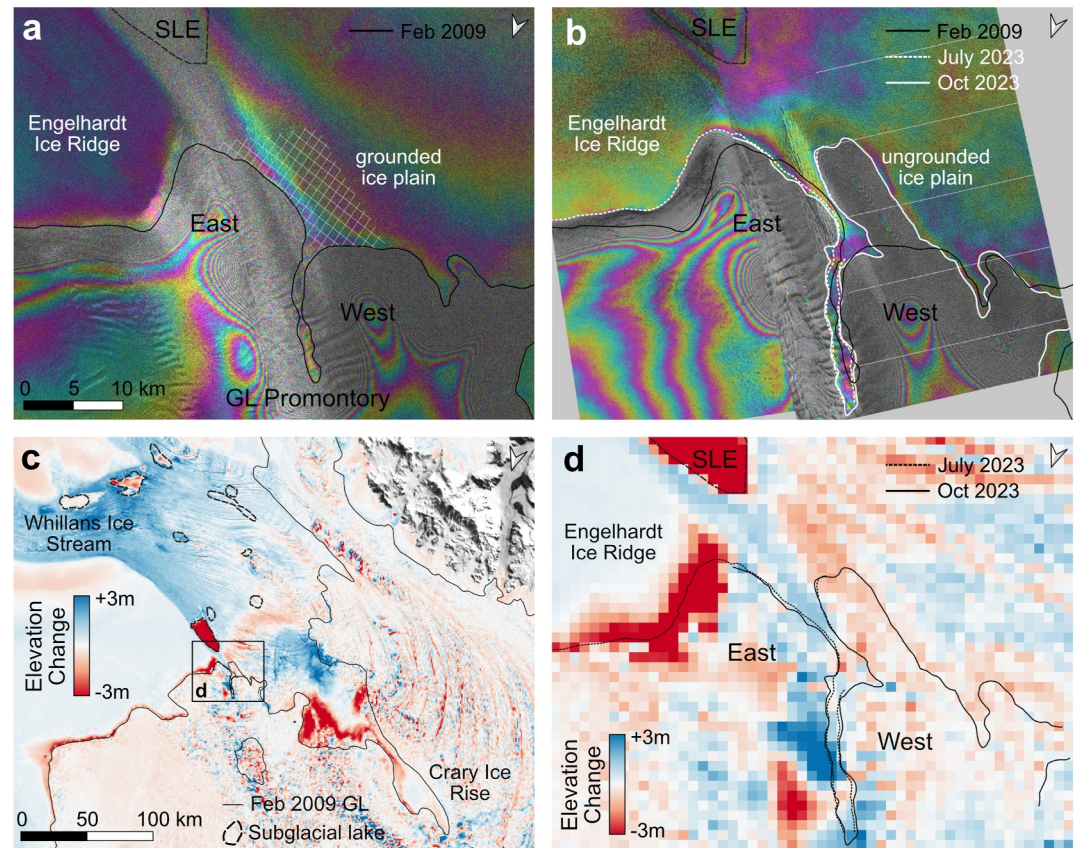


**Figure 6.** GL migration and surface elevation change downstream of SLE, 2009–24. (a) February 2009 RADARSAT-2 DInSAR and derived GL (black line) showing the east and west embayment and central grounded promontory. White hashed area shows the approx. location of the grounded ice plain identified in Brunt et al. (2010). (b) TerraSAR-X DInSAR and derived GLs from July to October 2023 (white dashed and solid lines, respectively; Marsh et al., 2024). (c) ICESat-2 ATL15 gridded surface elevation change across the wider Gould Coast, 2019–24 (Smith et al., 2024). (d) Zoom of (c) over the same region as (a) and (b) showing the 2023 GL positions.

*Timeline of ungrounding:* Given the sparse SAR coverage this far south and the absence of ICESat-2 data prior to 2019, it is difficult to precisely determine the timing of ice plain ungrounding and GL retreat. However, by combining all available satellite observations during this period, we have built a comprehensive timeline to constrain the evolution of the ungrounding from 2009 onwards as well as possible (Figure 8). The first two observations were RADARSAT-2 and TerraSAR-X DInSAR in 2009 and 2012, in which the absence of typical dense fringes over the ice plain indicate that the area was fully grounded (Figures 8a and 8b). By 2016, a weak tidal flexure signal in the TerraSAR-X DInSAR suggested that the ice plain was experiencing ephemeral grounding (Figure 8c; cf. Schmeltz et al., 2001). The next available observations are the first ICESat-2 RTLA measurements from May 2019 onwards, which show consistent evidence of tidal flexure and ungrounding where ground tracks cross the ice plain (Figure 8). Finally, in 2023, extensive fringes in the TerraSAR-X DInSAR images indicate that the whole ice plain was fully afloat (Figures 8e and 8f).

Overall, this timeline suggests that the main period of GL retreat and subsequent ice plain ungrounding in the west embayment occurred between 2016 and 2019. We can be confident that this is a real signal of GL retreat over this period rather than a product of tidal sampling or aliasing (e.g., Padman et al., 2018) based on the fact that the 2023 DInSAR sampled a lower maximum tidal amplitude and total tide range than in 2009 and 2012 (Table 1).

*ICESat-2 thinning rates:* The gridded ICESat-2 elevation change data show that the ice in the newly ungrounded ice plain thinned by  $\sim 0.5$ – $2$  m between 2019 and 2024 (Figure 6d). This region appears to connect to a wider “crescent” of thinning that extends further inland across Whillans Ice Plain to the western side of the Crary Ice Rise (Figure 6c), standing in contrast to the wider thickening trend of Whillans Ice Stream.



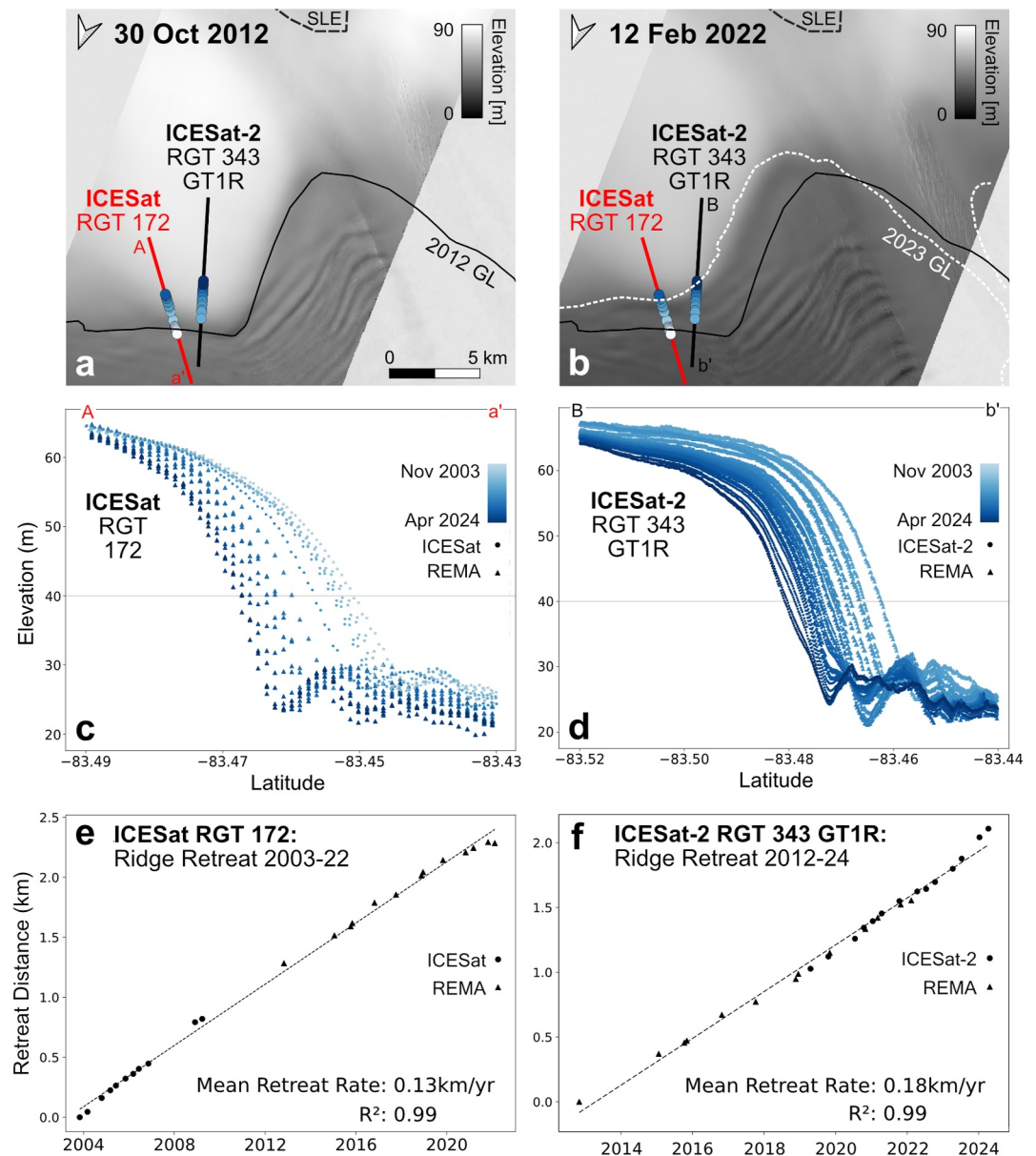


**Figure 7.** Engelhardt Ice Ridge retreat, 2003–24. (a and b) REMA DEM strips from 30 October 2012 and 12 February 2022 (Howat et al., 2019) showing the closest available DInSAR GL positions. Colored circles mark the location of the ridge at the 40-m elevation contour along ICESat track 172 (red) and ICESat-2 RGT 343 ground track 1R (GT1R) (black) for each of the sampled time stamps in (c and d). (c) Repeat surface elevation profiles along ICESat RGT 172, combining elevations from ICESat November 2003–March 2009 (circles) and elevations sampled along the same ground track from REMA DEM strips October 2012–February 2022 (triangles). (d) Repeat surface elevation profiles along ICESat-2 RGT 343 GT1R, combining elevations from ICESat-2 April 2019–April 2024 (circles) and elevations sampled along the same ground track from REMA DEM strips October 2012–February 2022 (triangles). (e and f) Ridge retreat distance at the 40-m elevation contour along: (e) ICESat RGT 172, November 2003–February 2022; and (f) ICESat-2 RGT 343 GT1R, October 2012–April 2024.

*ICESat-2 tidal flexure:* The ICESat-2 RTLA results show that there is considerable tidal flexure and tidal GL migration within the newly ungrounded ice plain (Figure 9). This is illustrated along RGT 23 GT2L (Figures 8a–8f), where the observed differences in the along-track elevation anomalies between repeat measurements on 26 March, 25 June, and 23 December 2021 reflect the change in the extent of tidal flexure and depth of seawater intrusion across the tidal cycle (Figure 9e). The maximum elevation anomaly across the ice plain (+0.8 m) was observed on 25 June, which was sampled immediately after a peak spring tide (Figure 9c). The ice plain was

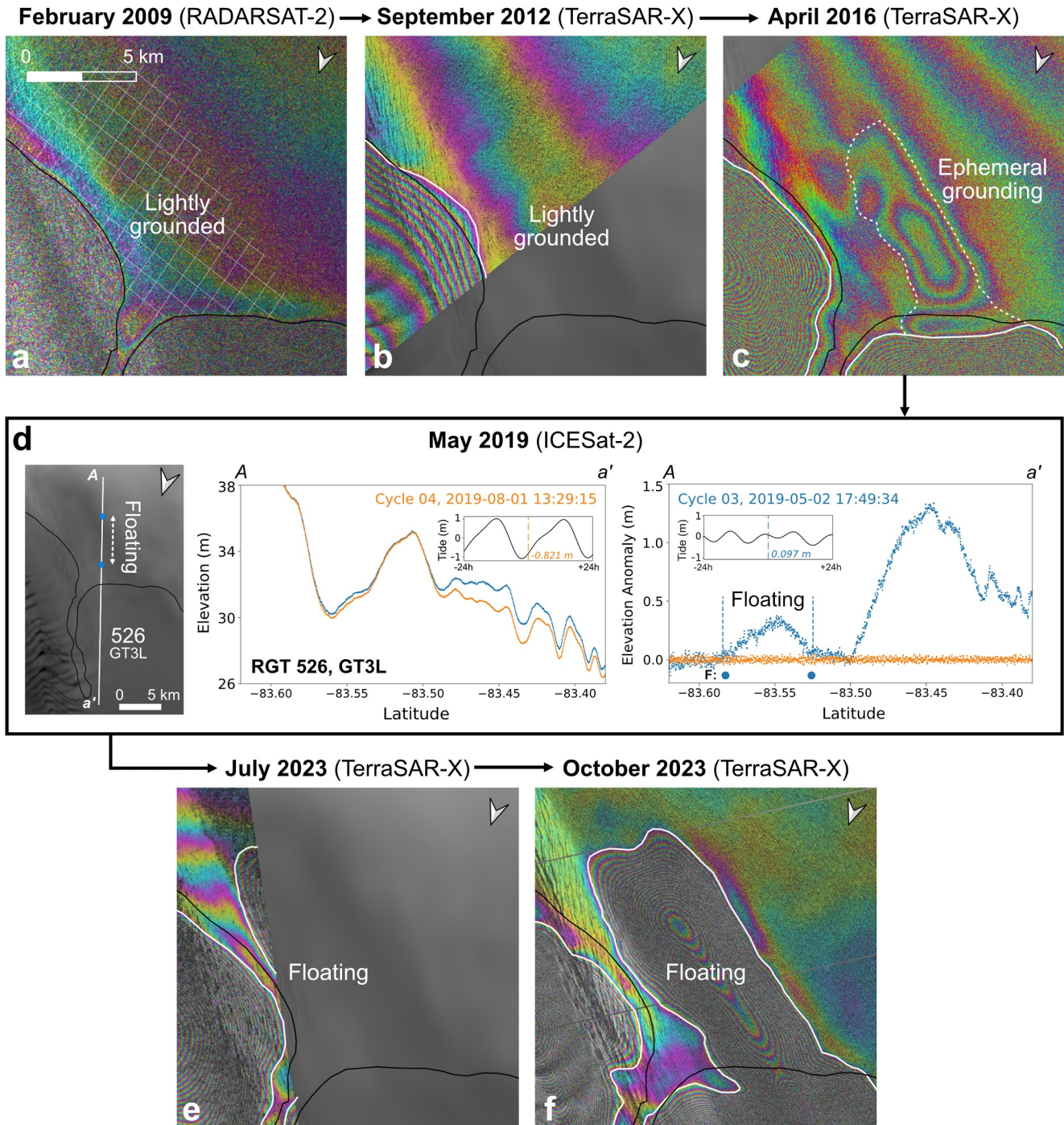


**Figure 8.** Timeline of GL retreat and ice plain ungrounding in the west embayment from a combination of RADARSAT-2 and TerraSAR-X DInSAR and ICESat-2 RTLA (Marsh et al., 2024). (a) February 2009; (b) September 2012; (c) April 2016 (weak signal of GL retreat marked with dashed white line); (d) May 2019, where ICESat-2 repeat elevation and elevation anomalies along RGT 526 GT3L show tidal flexure (i.e., ungrounding) over the section of the track crossing the ice plain; (e) July 2023; (f) October 2023. Black line shows the 2009 GL for comparison between images. The white hashed area in (a) shows the approximate location of the grounded ice plain identified in Brunt et al. (2010). The total expected vertical height difference for each DInSAR image is provided in Table 1.

sampled at lower tides on 26 March and 23 December (Figure 9e) and the smaller elevation anomalies on these dates (Figures 9b and 9d) indicate less tidal flexure and shallower water depths (Figures 9b and 9d). When the RTLA method was applied to all ICESat-2 tracks that cross the ungrounded ice plain (Figure 9g), we observed that the whole region is estuary-like (Horgan et al., 2013), widening and deepening at high tide and possibly re-



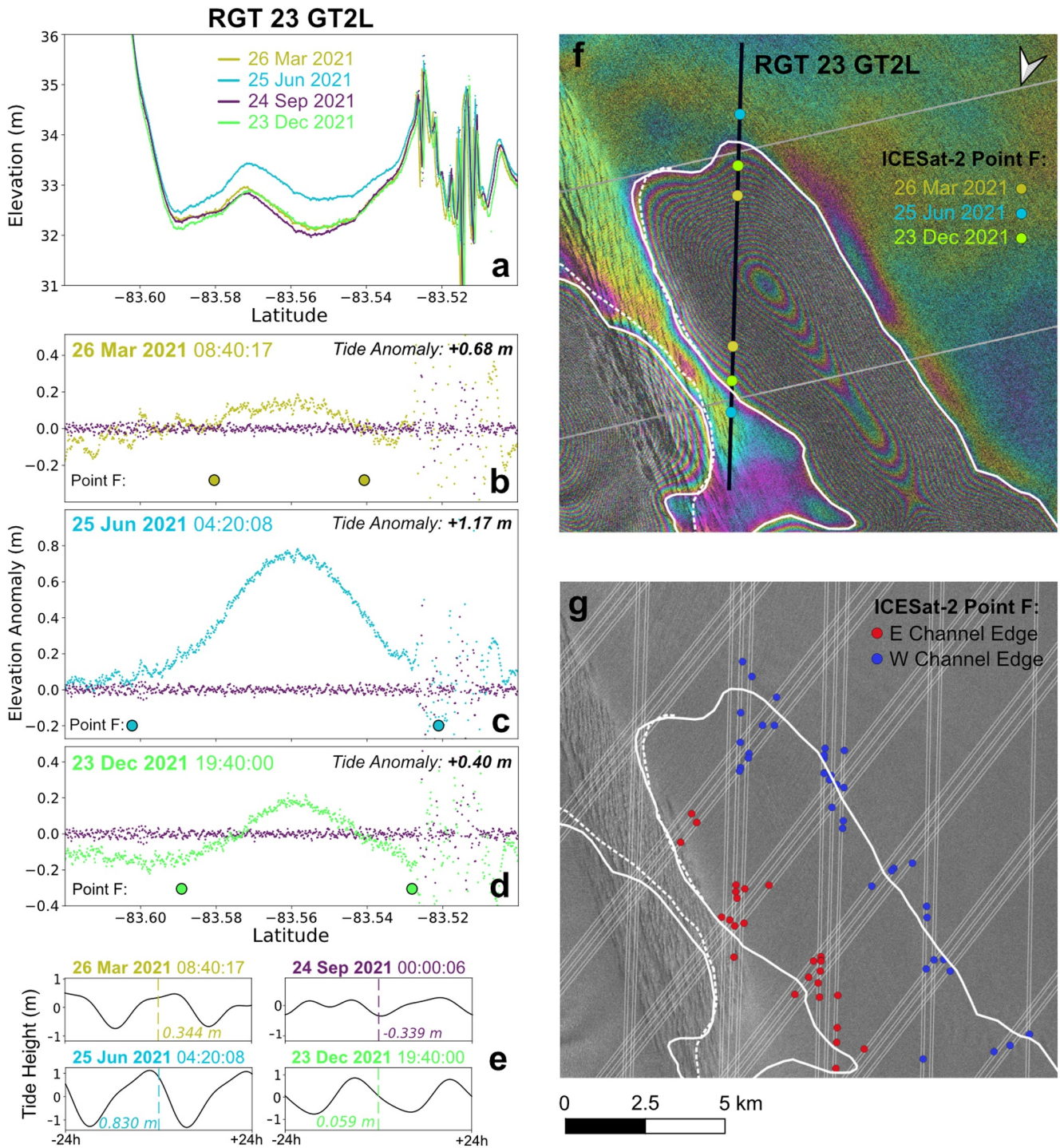


**Figure 9.** ICESat-2 RTLA measurements of tidal flexure and tidal GL migration within the newly ungrounded ice plain at the west embayment. (a) Repeat ATL06 surface elevation profiles along ICESat-2 RGT 23 GT2L from 26 March (gold), 25 June (blue), 24 September (purple) and 23 December (green) 2021 across the newly ungrounded ice plain (location in (f)). (b–d) ATL06 elevation anomalies from 26 March, 25 June and 23 December 2021, each calculated against the low tide reference profile of 24 September 2021 (purple). Derived Point F positions (inland limit of tidal flexure) for either side of the channel are shown by the colored dots along the x-axis. (e) Modeled tides 24 hr before and after each sampled ICESat-2 overpass, extracted from the Circum-Antarctic Tidal Simulation 2008 (CATS2008\_v2023; Howard et al., 2019) using the pyTMD software package (version 2.1.0., Sutterley et al., 2017). (f) Location of derived Point F positions for each date (colored dots) along ICESat-2 RGT 23 GT2L (solid black) overlain on the October 2023 TerraSAR-X DInSAR. (g) Point F positions along the western (blue) and eastern (red) edge of the newly ungrounded ice plain from all intersecting ICESat-2 RGTs, overlain on the TerraSAR-X multi-look backscatter image from 14 October 2023.

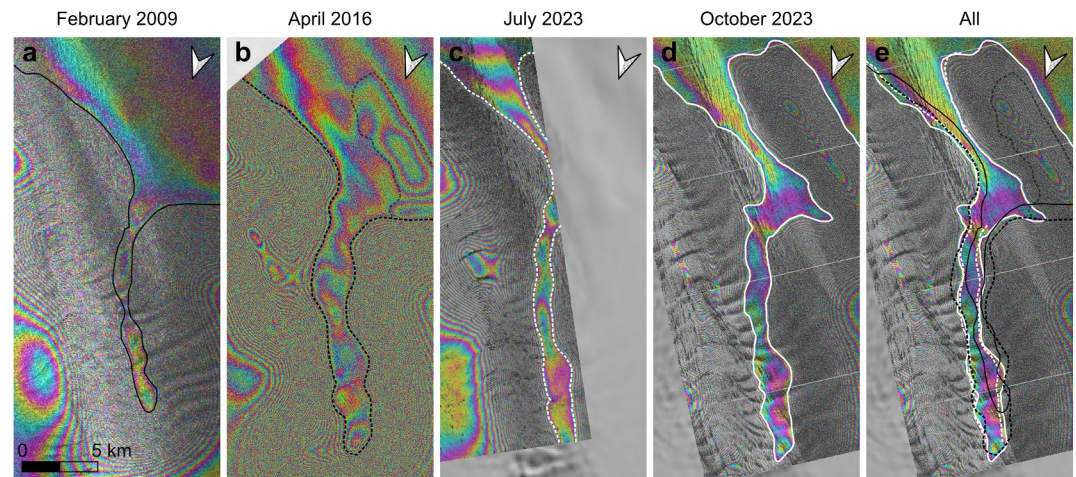


**Figure 10.** DInSAR time-series showing the change in the shape and length of the grounded promontory separating the east and west GL embayments. DInSAR fringes and delineated GL (Marsh et al., 2024) for four epochs: (a) February 2009 (RADARSAT-2); (b) April 2016 (TerraSAR-X); (c) July 2023 (TerraSAR-X); (d) October 2023 (TerraSAR-X). (e) All delineated GL positions overlain on the October 2023 (TerraSAR-X) DInSAR for comparison.

grounding at low tide. This is further evidenced by the tidal strand cracks visible in the TerraSAR-X backscatter imagery (Figure 5d).

#### 4.2.3. Grounded Promontory

The DInSAR time-series for the period 2009–23 also shows changes in the central grounded promontory that separates the east and west embayments (Figure 10), located in a region of localized ice thickening (Figure 6d). Over this time, this long and narrow feature oriented parallel to ice flow has migrated eastwards by  $\sim 1$  km and extended  $\sim 3$  km further seaward. There is evidence of increased surface damage around this feature, with prominent long-wavelength undulations and extensive crevassing (Figure 5c).

## 5. Discussion

### 5.1. Engelhardt Subglacial Lake (SLE) Drainage

The 2021–24 drainage of SLE occurred  $\sim 18$  years after the last drainage, representing the longest interval observed between successive drainages of the same subglacial lake in Antarctica. We estimate that this event discharged  $\sim 2.3$  km<sup>3</sup> of subglacial water into the RIS cavity over the 31 months to January 2024. This total drainage volume would have increased as drainage continued until at least April 2024, giving a total estimated drainage period of 34–36 months. The magnitude of surface subsidence over SLE from 2021–24 was at least 5 m greater than that observed during the 2003–06 drainage event (Figure 3c), which discharged an estimated  $\sim 2.0$  km<sup>3</sup> over a similar total time period of 33 months (Fricker et al., 2007). The higher spatial and temporal density of measurements from ICESat-2 has allowed us to delineate a more accurate lake boundary and track the activity of a newly identified upstream feeder lake (Figures 3 and 4).

The onset mechanism suggested for the 2003–06 SLE drainage was the breaching of a weak pressure barrier of  $\sim 50$  kPa that had kept the downstream end sealed off from the ocean (Fricker et al., 2007). As the lake filled, the rising pressure head reached  $\sim 100$ – $200$  kPa, breaching the ice seal to initiate drainage. We propose a similar onset mechanism for the 2021–24 drainage, except that the trigger for the seal breach was the pulse of subglacial water discharged from the newly identified upstream feeder lake in September 2020 (Figures 3 and 4). This “cascading drainage” behavior between interconnected lakes has been observed elsewhere in Antarctica (Fricker & Scambos, 2009; Fricker et al., 2014; Malczyk et al., 2020; Neckel et al., 2021; Siegfried et al., 2023). We note that drainage from the upstream feeder lake may have also initiated the 2003–06 SLE drainage, but we lack observations as it was not well-sampled by ICESat (Figure 3a).



The rate of surface subsidence measured by ICESat-2 accelerated as drainage progressed, reaching a maximum in July 2023 (Figures 3b, 3c, and 4t), likely coinciding with the evolution to a more efficient drainage system. Although we define the timing of drainage onset as when we first detected a decrease in surface elevation over the lake (July 2021), SLE may have begun “leaking” at slower rates several months beforehand. This has been proposed at subglacial lakes Mercer and Conway (Carter et al., 2013) and was modeled for the 2003–06 SLE drainage (Carter et al., 2017).

The outflow of  $>2.3 \text{ km}^3$  of freshwater from SLE drainage into the RIS cavity will affect the freshwater budget, local circulation and melt patterns in the cavity (Carter & Fricker, 2012; Gwyther et al., 2023; Hawkings et al., 2020; Nakayama et al., 2021). Basal melt rates at the Gould Coast GL are relatively low ( $\sim 0.05\text{--}1 \text{ m yr}^{-1}$ ; e.g., Catania et al., 2010; Dinniman et al., 2007; Holland et al., 2003; MacAyeal, 1984), but models indicate that this can increase by a factor of three at subglacial lake drainage outflows (Jenkins, 2011). Therefore, this drainage has the potential to accelerate localized ice thinning and GL retreat (Carter & Fricker, 2012; Pelle et al., 2023).

## 5.2. Revisiting the Relationship Between SLE Drainage and Grounding Line Retreat

Following the 2003–06 drainage of SLE, it remained an open question whether GL retreat had triggered the drainage or whether drainage caused the retreat (Fricker & Scambos, 2009). We revisit this question using the new high-resolution satellite observations made before and during the 2021–24 drainage event, considering the east and west embayments separately.

### 5.2.1. East Embayment

The GL retreat along Engelhardt Ice Ridge (Figure 7) in the east embayment continues a longer-term trend that has been observed since at least 1963 and is suggested to be linked to the deceleration of Whillans Ice Stream (Bindschadler & Vornberger, 1998; Fricker et al., 2007). We find no evidence of acceleration in GL retreat in this area following the onset of SLE drainage in July 2021 (Figures 7e and 7f), suggesting that retreat was not directly associated with the drainage. We also consider it unlikely that GL retreat was the primary trigger for the 2021 SLE drainage because the previous drainage event occurred when the GL was much further seaward. Although not the primary influence, we cannot rule out the possibility that GL retreat facilitated the onset of drainage by shortening the bridge of grounded ice between SLE and the RIS cavity, changing the ice surface slope and weakening the hydraulic seal (Hayden & Dow, 2023). This mechanism was proposed for a subglacial lake drainage beneath Crane Glacier in 2004–05 (Scambos et al., 2011).

### 5.2.2. West Embayment

The observation of 13 km of GL retreat in the west embayment is a substantial signal for the Gould Coast region. The extent of retreat appears to be controlled by the ice geometry, reaching the landward limit of the relatively thinner ice plain at the break-in-slope (Figures 6a, 6b, 8, and 9). Here, as across much of Whillans Ice Plain, the grounded ice sits close to hydrostatic equilibrium with low basal relief, meaning that small amounts of thinning can induce buoyancy-driven GL retreat (Batchelor et al., 2023; Carter et al., 2013; Catania et al., 2012). We suggest that the long-term, localized ice-sheet thinning observed by ICESat-2 inland of the west embayment GL (Figure 6d) has caused the ice plain to unground and the GL to retreat, following the ice plain life cycle of Brunt et al. (2011): from “lightly grounded” in 2009 to “ephemerally grounded” in 2016 and fully floating by 2023 (Figure 8). The cause of the localized thinning downstream of SLE, which contrasts with the more widespread ice dynamic thickening trend of Whillans Ice Stream (Smith et al., 2020), remains unclear. However, its location within the wider crescent of thinning extending to the southern side of Cray Ice Rise (Figure 6c) suggests it may be linked to larger-scale ice dynamics in the region (e.g., Beem et al., 2014; Siegfried et al., 2016). The ice plain ungrounding may also have been influenced by the complex stick-slip ice dynamics (Wiens et al., 2024; Winberry et al., 2009) and possible spatial variations in basal conditions (Christianson et al., 2016); however, these interpretations are limited by a lack of ground data (e.g., seismic or GPS) which would be necessary to obtain more detailed insights (e.g., Pratt et al., 2014; Siegfried et al., 2016; Winberry et al., 2014).

Our hypothesis that GL retreat in the west embayment was driven by the ungrounding of an ice plain due to long-term thinning suggests that it was unrelated to the 2021–24 SLE drainage event. This is supported by two key lines of evidence: (a) the timing of the observed GL retreat (2016–19; Figure 8) is uncorrelated with the drainage onset (2021; Figure 3); and (b) the modeled hydrological pathway (if correct) predicts that SLE should drain via the east

embayment (Figure 1b), where it would exert minimal influence on ice dynamics in the west embayment. However, given the proximity of SLE to the GL, it is unlikely that there was no interaction between the two processes. It is possible that SLE drainage accelerated the GL retreat, particularly if ice thinning and GL migration altered the hydropotential gradient (Carter et al., 2013) enough to re-direct the outflow from SLE via the west embayment. This could increase the localized basal melt rate at the GL (Carter & Fricker, 2012; Pelle et al., 2023; Whiteford et al., 2022), which together with tidal flows could drive further thinning and GL retreat (Horgan et al., 2013). It could also change the subglacial conditions—including basal slipperiness—upstream of the GL, influencing ice flow and GL retreat (Sergienko & Haseloff, 2023). Flow-switching of this kind has previously been proposed across Whillans Ice Plain (Carter et al., 2013; Marsh et al., 2016), but it is not possible to unequivocally verify without measurements from the ice shelf cavity.

### 5.2.3. Grounded Promontory

The grounded GL promontory separating the east and west embayments is another signature of interaction between subglacial hydrology and the GL. Based on its location, orientation, geometry and surface damage, we suggest that this may be the surface expression of local grounding of the ice on a ridge-like bedform. A CReSIS radar survey over the region (CReSIS, 2014) reveals there is a bump in the bed topography, but without drilling into the substrate, we cannot confirm its origin. Since it protrudes seaward by several kilometers, this bed feature is likely to impact localized ocean circulation patterns in the ice shelf cavity. We propose three possible origins of the ridge:

- (i) *Ice-stream lateral shear-moraine (ISLM)*: ISLMs are ridges of sediment (predominantly subglacial till) accumulated at ice stream shear margins, enhanced by the presence of subglacial meltwater (Batchelor & Dowdeswell, 2016; Hindmarsh & Stokes, 2008; Stokes & Clark, 2002). The location of the promontory along the Whillans Ice Stream shear margin, which is underlain by deformable till (Kamb, 2001) with a well-established supply of subglacial meltwater, is consistent with an ISLM.
- (ii) *Esker*: Eskers are the depositional evidence of a former subglacial meltwater channel, sometimes formed during subglacial lake outburst floods (Burke et al., 2008). Drews et al. (2017) proposed the first evidence from Antarctica of actively evolving eskers deposited by subglacial water conduits at the Roi Baudouin Ice Shelf GL. The extensive region of crevassing immediately upstream of the GZ promontory could offer additional evidence for this interpretation (Figure 5b). This surface feature has been observed in satellite imagery as early as 1989 (Bindschadler, 1993) and has continued to advect downstream with ice flow. Its origin is unknown, but it could be linked to past GL advancement or evidence of a former subglacial melt channel or collapsed lake. However, we note that eskers have been “notably absent” from the paleo-record in the Ross Sector (Greenwood et al., 2016).
- (iii) *Fault-controlled structure*: The subglacial ridge may represent the upper footwall of a half-graben formed by en-echelon faulting during a phase of crustal extension. Several such faults have been identified running parallel beneath the Ross Ice Shelf (e.g., Greischar et al., 1992; Munson & Bentley, 1992), including one that has been proposed to control the expression of Crary Ice Rise (Muto et al., 2013), which suggests it could be plausible for another to exist in this location.

Regardless of origin, the ~3 km lengthening of the promontory between 2009 and 2023 (Figure 10) is most likely the result of localized ice thickening (Figure 6d), which caused the ice to ground on a longer section of the existing bed feature, initiating a positive feedback of enhanced grounding, slow-down and thickening. It is possible that it was also affected by the enhanced sediment erosion, transport and deposition linked to SLE drainage (Carter et al., 2017; Horgan et al., 2013; Livingstone et al., 2019), although the relatively low mean drainage discharge rate ( $\sim 20 \text{ m}^3 \text{ s}^{-1}$ ) indicates that any sediment deposition was likely distributed over a substantial area. Depositional features at GLs can provide resistance to flow through lateral drag (Stokes & Clark, 2002) and have been proposed as possible mechanisms for GL stabilization in the paleo-record (Alley et al., 2007; Batchelor & Dowdeswell, 2016). Therefore, we suggest that this feature is of interest for future monitoring.

## 5.3. Implications of Grounding Line Retreat

### 5.3.1. Seawater Intrusion

The newly ungrounded tidally modulated estuary in the west embayment shows similarities to those observed at the GLs of Amery (Chen et al., 2023) and Totten (Li et al., 2023), and provides a new route for ocean water to flush in



and out of the GZ cavity (Horgan et al., 2013). Assuming that the ice plain is grounded during low tide, we estimate that the maximum depth of tidal seawater intrusion beneath the ice plain is <1 m at high tide (Figure 9g). These intrusions can reduce basal friction (e.g., Anandakrishnan et al., 2003), affect cavity circulation and enhance basal melt rates (Makinson et al., 2011; Milillo et al., 2019; Robel et al., 2022). Such complex and small-scale ice-ocean interactions have been proposed as a key missing piece in ice sheet models (Rignot, 2023) but are challenging to observe. At SLE this has only been possible as a result of the increased temporal sampling and coverage of ICESat-2, but our ability to fully characterize this behavior (which would include confirming the flotation state of the ice plain at low tide) would be improved in future by the collection of in situ observations or higher-frequency DInSAR acquisitions (e.g., from COSMO-SkyMed; Brancato et al., 2020; Milillo et al., 2017, 2019 or other SAR systems and constellations including the future NISAR mission). We note, however, that these signals are extremely complex to interpret as the region is likely subject to bridging stresses and flexural limits imposed by the geometry, incomplete tidal circulation and lags between rising and falling tides (e.g., Freer et al., 2023).

### 5.3.2. Future Evolution

Improving projections of future ice loss in Antarctica relies on a better understanding of key processes, including how the GL responds to different forcing mechanisms. Subglacial hydrology upstream of the GL has remained one of the least understood forcings, in part due to a scarcity of observations. The 2021–24 drainage of SLE, as one of the only known active subglacial lakes in Antarctica within 10 km of the GL, presented a rare opportunity to study these processes in close proximity, taking advantage of the improvements in spatial and temporal resolution and coverage of satellite data sets since its last drainage two decades previously.

Although the current satellite evidence does not show a direct causal link between lake drainage and GL retreat over this distance, it is possible that a link will develop as the GL continues to retreat toward the lake. If retreat downstream of SLE continues at current rates, the GL in the east embayment could connect with SLE within 40 years, and even sooner in the west embayment. This connection would link SLE with the RIS cavity, affecting local ice and lake dynamics and the overall shape of Whillans Ice Plain. Elsewhere in Antarctica, subglacial lakes have been observed within 40 km of the GL at Whillans and Mercer (Figure 1a), Kamb, MacAyeal, Rutford, Totten, and Thwaites (Malczyk et al., 2020; Siegfried & Fricker, 2018) and within 10 km at Pine Island Glacier (Joughin et al., 2016). Together, these ice streams drain 15–20% of the Antarctic ice sheet (Rignot et al., 2019). Understanding if and how their dynamics may be influenced in the future by subglacial hydrology (particularly the fill-and-drain of active subglacial lakes) is an important question, especially in regions subject to rapid GL retreat such as Totten, Pine Island and Thwaites (Li et al., 2023; Milillo et al., 2019), where the distance between the GL and subglacial lakes is shortening.

## 6. Summary

We have presented a 21-year record of satellite-derived surface elevation change at Engelhardt Subglacial Lake (SLE) in West Antarctica, which includes the latest drainage event from 2021 to 2024. Between July 2021 and April 2024, the ice surface over SLE lowered by up to 15 m, draining more than 2.3 km<sup>3</sup> of subglacial water into the Ross Ice Shelf cavity. Over the same period, we have observed significant evolution of the downstream grounding zone (GZ), including 2–3 km of grounding line (GL) retreat along Engelhardt Ice Ridge since 2009, and 13 km of GL retreat in the west embayment where an ice plain has ungrounded.

Analysis of the satellite observations from the 2021–24 drainage indicates that SLE drainage and GL retreat were largely independent processes: drainage was initiated by the influx of water from a smaller upstream feeder lake; GL retreat in the east embayment was mainly driven by the long-term retreat of Engelhardt Ice Ridge; and GL retreat in the west embayment was due to long-term dynamic ice thinning that caused the lightly grounded ice plain to reach flotation. However, we acknowledge that there are unobserved mechanisms by which these processes could have influenced each other. For example, the outflow from SLE drainage could increase basal melt in the GZ, thus accelerating thinning and enhancing GL retreat. Additionally, GL retreat would reduce the distance between the lake and the ice shelf, affecting the ice surface slope, which could weaken the hydraulic seal sufficiently to facilitate the onset of drainage.

Our observation of an approximately 27 km long and 2 km wide subglacial bedform protruding seaward from the GL poses additional questions about the relationship between subglacial hydrology and the GL. Its identity and exact formation mechanism is not known, but we believe it may be the surface expression of an ice-stream lateral

shear-moraine, esker, or a fault-controlled structure. We suggest that its ~3 km lengthening since 2009 may be due to localized ice thickening causing grounding on more of the existing bed feature, possibly enhanced by sediment outflow from SLE drainage.

Overall, our observations highlight the complex interactions between ice dynamics, subglacial hydrology and sediment transport in Antarctic GZs. The new high-resolution satellite data have allowed us to resolve these behaviors much better than in the past, but there are still gaps in our understanding. We suggest that this region is important for examining a variety of dynamic GZ processes—with opportunities for monitoring using a combination of satellite remote sensing (including the upcoming NISAR mission), airborne surveys and drilling campaigns.

## Data Availability Statement

The ICESat-2 ATL06 L3A Land Ice Height (version 6) data used for measuring surface elevation change and grounding line position 2019–24 are available at the National Snow and Ice Data Center (NSIDC) (Smith et al., 2023). The ICESat-2 ATL15 L3B Gridded Antarctic Land Ice Height Change (version 3) data used for measuring surface elevation change 2019–24 are available at NSIDC (Smith et al., 2024). The ICESat GLAS/ICESat L1B Global Elevation Data (HDF5) (version 34) data used for measuring surface elevation change 2003–09 are available at NSIDC (Zwally et al., 2014). The swath-processed CryoSat-2 elevation data (Gourmelen et al., 2018) used for measuring surface elevation change 2010–20 were provided by the ESA CryoTempo-EOLIS project (<https://cryotempo-eolis.org>). The derived TerraSAR-X interferograms and derived GLs from 2012, 2016, and 2023 are published with the UK Polar Data Centre (Marsh et al., 2024). The derived hydrological flow pathways beneath Whillans Ice Stream are published with the UK Polar Data Centre (Sauthoff & Freer, 2024). The MEaSURES grounding line product (version 2) used to show the 2009 grounding line position is available at NSIDC (Rignot et al., 2016). The Reference Elevation Model of Antarctica (REMA) digital elevation model (DEM) mosaic (version 2) and strip (version 4.1) products used to measure the retreat of Engelhardt Ice Ridge are available at the Polar Geospatial Center (Howat et al., 2019).

## References

- Alley, R. B., Anandakrishnan, S., Dupont, T. K., Parizek, B. R., & Pollard, D. (2007). Effect of sedimentation on ice-sheet grounding-line stability. *Science*, 315(5820), 1838–1841. <https://doi.org/10.1126/science.1138396>
- Anandakrishnan, S., Voigt, D. E., Alley, R. B., & King, M. A. (2003). Ice stream D flow speed is strongly modulated by the tide beneath the Ross Ice Shelf. *Geophysical Research Letters*, 30(7), 1361. <https://doi.org/10.1029/2002GL016329>
- Bartos, M. (2020). Pysheds: Simple and fast watershed delineation in python. <https://doi.org/10.5281/zenodo.3822494>
- Batchelor, C. L., Christie, F. D. W., Ottesen, D., Montelli, A., Evans, J., Dowdeswell, E. K., et al. (2023). Rapid, buoyancy-driven ice-sheet retreat of hundreds of metres per day. *Nature*, 617(7959), 105–110. <https://doi.org/10.1038/s41586-023-05876-1>
- Batchelor, C. L., & Dowdeswell, J. A. (2016). Lateral shear-moraines and lateral marginal-moraines of palaeo-ice streams. *Quaternary Science Reviews*, 151, 1–26. <https://doi.org/10.1016/j.quascirev.2016.08.020>
- Beem, L. H., Tulaczyk, S. M., King, M. A., Bougamont, M., Fricker, H. A., & Christoffersen, P. (2014). Variable deceleration of Whillans Ice Stream, West Antarctica. *Journal of Geophysical Research: Earth Surface*, 119(2), 212–224. <https://doi.org/10.1002/2013JF002958>
- Bindschadler, R. (1993). Siple coast project research of Cray Ice Rise and the mouths of Ice Streams B and C, West Antarctica: Review and new perspectives. *Journal of Glaciology*, 39(133), 538–552. <https://doi.org/10.3189/S0022143000016439>
- Bindschadler, R., & Vormberger, P. (1998). Changes in the West Antarctic Ice Sheet since 1963 from declassified satellite photography. *Science*, 279(5351), 689–692. <https://doi.org/10.1126/science.279.5351.689>
- Borsa, A. A., Moholdt, G., Fricker, H. A., & Brunt, K. M. (2014). A range correction for ICESat and its potential impact on ice-sheet mass balance studies. *The Cryosphere*, 8(2), 345–357. <https://doi.org/10.5194/tc-8-345-2014>
- Brancato, V., Rignot, E., Milillo, P., Morlighem, M., Mouginot, J., An, L., et al. (2020). Grounding line retreat of Denman Glacier, East Antarctica, measured with COSMO-SkyMed radar interferometry data. *Geophysical Research Letters*, 47(7), e2019GL086291. <https://doi.org/10.1029/2019GL086291>
- Brunt, K. M., Fricker, H. A., & Padman, L. (2011). Analysis of ice plains of the Filchner–Ronne Ice Shelf, Antarctica, using ICESat laser altimetry. *Journal of Glaciology*, 57(205), 965–975. <https://doi.org/10.3189/002214311798043753>
- Brunt, K. M., Fricker, H. A., Padman, L., Scambos, T. A., & O’Neel, S. (2010). Mapping the grounding zone of the Ross Ice Shelf, Antarctica, using ICESat laser altimetry. *Annals of Glaciology*, 51(55), 71–79. <https://doi.org/10.3189/172756410791392790>
- Burke, M. J., Woodward, J., Russell, A. J., Fleisher, P. J., & Bailey, P. (2008). Controls on the sedimentary architecture of a single event englacial esker: Skeiðarárjökull, Iceland. *Quaternary Science Reviews*, 27(19–20), 1829–1847. <https://doi.org/10.1016/j.quascirev.2008.06.012>
- Carter, S. P., & Fricker, H. A. (2012). The supply of subglacial meltwater to the grounding line of the Siple Coast, West Antarctica. *Annals of Glaciology*, 53(60), 267–280. <https://doi.org/10.3189/2012AoG60A119>
- Carter, S. P., Fricker, H. A., & Siegfried, M. R. (2013). Evidence of rapid subglacial water piracy under Whillans Ice Stream, West Antarctica. *Journal of Glaciology*, 59(218), 1147–1162. <https://doi.org/10.3189/2013JoG13J085>
- Carter, S. P., Fricker, H. A., & Siegfried, M. R. (2017). Antarctic subglacial lakes drain through sediment-floored canals: Theory and model testing on real and idealized domains. *The Cryosphere*, 11(1), 381–405. <https://doi.org/10.5194/tc-11-381-2017>
- Catania, G., Hulbe, C., & Conway, H. (2010). Grounding-line basal melt rates determined using radar-derived internal stratigraphy. *Journal of Glaciology*, 56(197), 545–554. <https://doi.org/10.3189/002214310792447842>

- Catania, G., Hulbe, C., Conway, H., Scambos, T. A., & Raymond, C. F. (2012). Variability in the mass flux of the Ross ice streams, West Antarctica, over the last millennium. *Journal of Glaciology*, 58(210), 741–752. <https://doi.org/10.3189/2012JG11J219>
- Chen, H., Rignot, E., Scheuchl, B., & Ehrenfeucht, S. (2023). Grounding zone of Amery Ice Shelf, Antarctica, from differential synthetic-aperture radar interferometry. *Geophysical Research Letters*, 50(6), e2022GL102430. <https://doi.org/10.1029/2022GL102430>
- Christianson, K., Jacobel, R. W., Horgan, H. J., Alley, R. B., Anandakrishnan, S., Holland, D. M., & DallaSanta, K. J. (2016). Basal conditions at the grounding zone of Whillans Ice Stream, West Antarctica, from ice-penetrating radar. *Journal of Geophysical Research: Earth Surface*, 121(11), 1954–1983. <https://doi.org/10.1002/2015JF003806>
- CRISIS. (2014). *CRISIS radar depth sounder MCoRDS 4 data*. Digital Media. Retrieved from <http://data.cresis.ku.edu/>
- De Fleurian, B., Werder, M. A., Beyer, S., Brinkerhoff, D. J., Delaney, I., Dow, C. F., et al. (2018). SHMIP the subglacial hydrology model intercomparison Project. *Journal of Glaciology*, 64(248), 897–916. <https://doi.org/10.1017/jog.2018.78>
- Dinniman, M. S., Klinck, J. M., & Smith, W. O., Jr. (2007). Influence of sea ice cover and icebergs on circulation and water mass formation in a numerical circulation model of the Ross Sea, Antarctica. *Journal of Geophysical Research*, 112(C11), C11013. <https://doi.org/10.1029/2006JC004036>
- Drews, R., Pattyn, F., Hewitt, I. J., Ng, F. S. L., Berger, S., Matsuoka, K., et al. (2017). Actively evolving subglacial conduits and eskers initiate ice shelf channels at an Antarctic grounding line. *Nature Communications*, 8(1), 15228. <https://doi.org/10.1038/ncomms15228>
- Freer, B. I. D., Marsh, O. J., Hogg, A. E., Fricker, H. A., & Padman, L. (2023). Modes of Antarctic tidal grounding line migration revealed by Ice, Cloud, and land Elevation Satellite-2 (ICESat-2) laser altimetry. *The Cryosphere*, 17(9), 4079–4101. <https://doi.org/10.5194/tc-17-4079-2023>
- Fretwell, P., Pritchard, H. D., Vaughan, D. G., Bamber, J. L., Barrand, N. E., Bell, R., et al. (2013). Bedmap2: Improved ice bed, surface and thickness datasets for Antarctica. *The Cryosphere*, 7(1), 375–393. <https://doi.org/10.5194/tc-7-375-2013>
- Fricker, H. A., Carter, S. P., Bell, R. E., & Scambos, T. (2014). Active lakes of Recovery Ice Stream, East Antarctica: A bedrock-controlled subglacial hydrological system. *Journal of Glaciology*, 60(223), 1015–1030. <https://doi.org/10.3189/2014JG14J063>
- Fricker, H. A., & Scambos, T. (2009). Connected subglacial lake activity on lower Mercer and Whillans Ice Streams, West Antarctica, 2003–2008. *Journal of Glaciology*, 55(190), 303–315. <https://doi.org/10.3189/002214309788608813>
- Fricker, H. A., Scambos, T., Bindschadler, R., & Padman, L. (2007). An active subglacial water system in West Antarctica mapped from space. *Science*, 315(5818), 1544–1548. <https://doi.org/10.1126/science.1136897>
- Fricker, H. A., Siegfried, M. R., Carter, S. P., & Scambos, T. A. (2016). A decade of progress in observing and modelling Antarctic subglacial water systems. *Philosophical Transactions of the Royal Society A: Mathematical, Physical & Engineering Sciences*, 374(2059), 20140294. <https://doi.org/10.1098/rsta.2014.0294>
- Fried, M. J., Hulbe, C. L., & Fahnestock, M. A. (2014). Grounding-line dynamics and margin lakes. *Annals of Glaciology*, 55(66), 87–96. <https://doi.org/10.3189/2014AoG66A216>
- Gourmelen, N., Escorihuela, M. J., Shepherd, A., Foresta, L., Muir, A., Garcia-Mondéjar, A., et al. (2018). CryoSat-2 swath interferometric altimetry for mapping ice elevation and elevation change. *Advances in Space Research*, 62(6), 1226–1242. <https://doi.org/10.1016/j.asr.2017.11.014>
- Greenwood, S. L., Clason, C. C., Helanow, C., & Margold, M. (2016). Theoretical, contemporary observational and palaeo-perspectives on ice sheet hydrology: Processes and products. *Earth-Science Reviews*, 155, 1–27. <https://doi.org/10.1016/j.earscirev.2016.01.010>
- Greischar, L. L., Bentley, C. R., & Whiting, L. R. (1992). An analysis of gravity measurements on the Ross Ice Shelf, Antarctica. In D. H. Elliot (Ed.), *Contributions to Antarctic research III, Antarctic research series* (Vol. 57, pp. 105–155). American Geophysical Union. <https://doi.org/10.1029/ar057p0105>
- Gudmundsson, G. H., Paolo, F. S., Adusumilli, S., & Fricker, H. A. (2019). Instantaneous Antarctic ice sheet mass loss driven by thinning ice shelves. *Geophysical Research Letters*, 46(23), 13903–13909. <https://doi.org/10.1029/2019GL085027>
- Gwyther, D. E., Dow, C. F., Jendersie, S., Gourmelen, N., & Galton-Fenzi, B. K. (2023). Subglacial freshwater drainage increases simulated basal melt of the Totten Ice Shelf. *Geophysical Research Letters*, 50(12), e2023GL103765. <https://doi.org/10.1029/2023GL103765>
- Hawkings, J. R., Skidmore, M. L., Wadham, J. L., Prisco, J. C., Morton, P. L., Hatton, J. E., et al. (2020). Enhanced trace element mobilization by Earth's ice sheets. *Proceedings of the National Academy of Sciences of the United States of America*, 117(50), 31648–31659. <https://doi.org/10.1073/pnas.2014378117>
- Hayden, A.-M., & Dow, C. F. (2023). Examining the effect of ice dynamic changes on subglacial hydrology through modelling of a synthetic Antarctic glacier. *Journal of Glaciology*, 1–14. <https://doi.org/10.1017/jog.2023.65>
- Hindmarsh, R. C. A., & Stokes, C. R. (2008). Formation mechanisms for ice-stream lateral shear margin moraines. *Earth Surface Processes and Landforms*, 33(4), 610–626. <https://doi.org/10.1002/esp.1665>
- Holland, D. M., Jacobs, S. S., & Jenkins, A. (2003). Modelling the ocean circulation beneath the Ross Ice Shelf. *Antarctic Science*, 15(1), 13–23. <https://doi.org/10.1017/S0954102003001019>
- Horgan, H. J., Alley, R. B., Christianson, K., Jacobel, R. W., Anandakrishnan, S., Muto, A., et al. (2013). Estuaries beneath ice sheets. *Geology*, 41(11), 1159–1162. <https://doi.org/10.1130/G34654.1>
- Horgan, H. J., & Anandakrishnan, S. (2006). Static grounding lines and dynamic ice streams: Evidence from the Siple Coast, West Antarctica. *Geophysical Research Letters*, 33(18), L18502. <https://doi.org/10.1029/2006GL027091>
- Howard, S. L., Padman, L., & Erofeeva, S. Y. (2019). CATS2008: Circum-Antarctic tidal simulation version 2008 (version 1) [Software]. *U.S. Antarctic Program (USAP) Data Center*. <https://doi.org/10.15784/601235>
- Howat, I. M., Porter, C., Smith, B. E., Noh, M.-J., & Morin, P. (2019). The reference elevation model of Antarctica. *The Cryosphere*, 13(2), 665–674. <https://doi.org/10.5194/tc-13-665-2019>
- Intergovernmental Panel on Climate Change (IPCC). (2023). Ocean, cryosphere and sea level change. In *Climate Change 2021—The Physical Science Basis: Working Group I Contribution to the Sixth Assessment Report of the Intergovernmental Panel on Climate Change* (pp. 1211–1362). Cambridge University Press. <https://doi.org/10.1017/9781009157896.011>
- Jenkins, A. (2011). Convection-driven melting near the grounding lines of ice shelves and tidewater glaciers. *Journal of Physical Oceanography*, 41(12), 2279–2294. <https://doi.org/10.1175/JPO-D-11-03.1>
- Joughin, I., Shean, D. E., Smith, B. E., & Dutrieux, P. (2016). Grounding line variability and subglacial lake drainage on Pine Island Glacier, Antarctica. *Geophysical Research Letters*, 43(17), 9093–9102. <https://doi.org/10.1002/2016GL070259>
- Kamb, B. (2001). Basal zone of the West Antarctic ice streams and its role in lubrication of their rapid motion. In *The West Antarctic ice sheet: Behavior and environment* (pp. 157–199). American Geophysical Union (AGU). <https://doi.org/10.1029/AR077p0157>
- Li, T., Dawson, G. J., Chuter, S. J., & Bamber, J. L. (2023). Grounding line retreat and tide-modulated ocean channels at Moscow University and Totten Glacier ice shelves, East Antarctica. *The Cryosphere*, 17(2), 1003–1022. <https://doi.org/10.5194/tc-17-1003-2023>

- Livingstone, S. J., Sole, A. J., Storrar, R. D., Harrison, D., Ross, N., & Bowling, J. (2019). Brief communication: Subglacial lake drainage beneath Isunguata Sermia, West Greenland: Geomorphic and ice dynamic effects. *The Cryosphere*, *13*(10), 2789–2796. <https://doi.org/10.5194/tc-13-2789-2019>
- MacAyeal, D. R. (1984). Thermohaline circulation below the Ross Ice Shelf: A consequence of tidally induced vertical mixing and basal melting. *Journal of Geophysical Research*, *89*(C1), 597–606. <https://doi.org/10.1029/JC089iC01p00597>
- Magruder, L., Brunt, K., Neumann, T., Klotz, B., & Alonzo, M. (2021). Passive ground-based optical techniques for monitoring the on-orbit ICESat-2 altimeter geolocation and footprint diameter. *Earth and Space Science*, *8*(10), e2020EA001414. <https://doi.org/10.1029/2020EA001414>
- Makinson, K., Holland, P. R., Jenkins, A., Nicholls, K. W., & Holland, D. M. (2011). Influence of tides on melting and freezing beneath Filchner-Ronne Ice Shelf, Antarctica. *Geophysical Research Letters*, *38*(6), L06601. <https://doi.org/10.1029/2010GL046462>
- Malczyk, G., Gourmelen, N., Goldberg, D., Wuite, J., & Nagler, T. (2020). Repeat Subglacial Lake drainage and filling beneath Thwaites Glacier. *Geophysical Research Letters*, *47*(23), e2020GL089658. <https://doi.org/10.1029/2020GL089658>
- Marsh, O. J., Floricioiu, D., & Freer, B. (2024). Double-difference TerraSAR-X interferograms and derived grounding lines at the grounding line of the Kamb and Whillans Ice Streams, West Antarctica, 2012–2023 (version 1.0) [Dataset]. *NERC EDS UK Polar Data Centre*. <https://doi.org/10.5285/e1d182b1-6aa6-434e-9390-f7956227cb82>
- Marsh, O. J., Fricker, H. A., Siegfried, M. R., Christianson, K., Nicholls, K. W., Corr, H. F. J., & Catania, G. (2016). High basal melting forming a channel at the grounding line of Ross Ice Shelf, Antarctica. *Geophysical Research Letters*, *43*(1), 250–255. <https://doi.org/10.1002/2015GL066612>
- McMillan, M., Corr, H., Shepherd, A., Ridout, A., Laxon, S., & Cullen, R. (2013). Three-dimensional mapping by CryoSat-2 of subglacial lake volume changes. *Geophysical Research Letters*, *40*(16), 4321–4327. <https://doi.org/10.1002/grl.50689>
- McMillan, M., Shepherd, A., Sundal, A., Briggs, K., Muir, A., Ridout, A., et al. (2014). Increased ice losses from Antarctica detected by CryoSat-2. *Geophysical Research Letters*, *41*(11), 3899–3905. <https://doi.org/10.1002/2014GL060111>
- Milillo, P., Rignot, E., Mougino, J., Scheuchl, B., Morlighem, M., Li, X., & Salzer, J. T. (2017). On the short-term grounding zone dynamics of Pine Island Glacier, West Antarctica, observed with COSMO-SkyMed interferometric data: PIG grounding line dynamics. *Geophysical Research Letters*, *44*(20), 10436–10444. <https://doi.org/10.1002/2017GL074320>
- Milillo, P., Rignot, E., Rizzoli, P., Scheuchl, B., Mougino, J., Bueso-Bello, J., & Prats-Iraola, P. (2019). Heterogeneous retreat and ice melt of Thwaites Glacier, West Antarctica. *Science Advances*, *5*(1), eaau3433. <https://doi.org/10.1126/sciadv.aau3433>
- Morlighem, M., Rignot, E., Binder, T., Blankenship, D., Drews, R., Eagles, G., et al. (2020). Deep glacial troughs and stabilizing ridges unveiled beneath the margins of the Antarctic ice sheet. *Nature Geoscience*, *13*(2), 132–137. <https://doi.org/10.1038/s41561-019-0510-8>
- Munson, C. G., & Bentley, C. R. (1992). The crustal structure beneath ice stream C and ridge BC, West Antarctica from seismic refraction and gravity measurements. In Y. Yoshida, K. Kaminuma, & K. Shiraiishi (Eds.), *Recent progress in Antarctic Earth science* (pp. 507–514). TERRAPUB.
- Muto, A., Christianson, K., Horgan, H. J., Anandakrishnan, S., & Alley, R. B. (2013). Bathymetry and geological structures beneath the Ross Ice Shelf at the mouth of Whillans Ice Stream, West Antarctica, modeled from ground-based gravity measurements. *Journal of Geophysical Research: Solid Earth*, *118*(8), 4535–4546. <https://doi.org/10.1002/jgrb.50315>
- Nakayama, Y., Cai, C., & Seroussi, H. (2021). Impact of subglacial freshwater discharge on Pine Island Ice Shelf. *Geophysical Research Letters*, *48*(18), e2021GL093923. <https://doi.org/10.1029/2021GL093923>
- Neckel, N., Franke, S., Helm, V., Drews, R., & Jansen, D. (2021). Evidence of cascading subglacial water flow at Jutulstraumen Glacier (Antarctica) derived from Sentinel-1 and ICESat-2 measurements. *Geophysical Research Letters*, *48*(20), e2021GL094472. <https://doi.org/10.1029/2021GL094472>
- Padman, L., Siegfried, M. R., & Fricker, H. A. (2018). Ocean tide influences on the Antarctic and Greenland Ice Sheets. *Reviews of Geophysics*, *56*(1), 142–184. <https://doi.org/10.1002/2016RG000546>
- Paterson, W. S. B. (1994). *Physics of glaciers* (3rd ed.). Pergamon.
- Pelle, T., Greenbaum, J. S., Dow, C. F., Jenkins, A., & Morlighem, M. (2023). Subglacial discharge accelerates future retreat of Denman and Scott Glaciers, East Antarctica. *Science Advances*, *9*(43), eadi9014. <https://doi.org/10.1126/sciadv.adi9014>
- Pratt, M. J., Winberry, J. P., Wiens, D. A., Anandakrishnan, S., & Alley, R. B. (2014). Seismic and geodetic evidence for grounding-line control of Whillans Ice Stream stick-slip events. *Journal of Geophysical Research: Earth Surface*, *119*(2), 333–348. <https://doi.org/10.1002/2013JF002842>
- Priscu, J. C., Kalin, J., Winans, J., Campbell, T., Siegfried, M. R., Skidmore, M., et al. (2021). Scientific access into Mercer Subglacial Lake: Scientific objectives, drilling operations and initial observations. *Annals of Glaciology*, *62*(85–86), 340–352. <https://doi.org/10.1017/aog.2021.10>
- Rignot, E. (2023). Observations of grounding zones are the missing key to understand ice melt in Antarctica. *Nature Climate Change*, *13*(10), 1010–1013. <https://doi.org/10.1038/s41558-023-01819-w>
- Rignot, E., Mougino, J., & Scheuchl, B. (2011). Antarctic grounding line mapping from differential satellite radar interferometry. *Geophysical Research Letters*, *38*(10). <https://doi.org/10.1029/2011GL047109>
- Rignot, E., Mougino, J., & Scheuchl, B. (2016). MEaSUREs Antarctic grounding line from differential satellite radar interferometry (version 2) [Dataset]. *NASA National Snow and Ice Data Center Distributed Active Archive Center*. <https://doi.org/10.5067/IKBWW4RYHF1Q>
- Rignot, E., Mougino, J., & Scheuchl, B. (2017). MEaSUREs InSAR-based Antarctica ice velocity Map (version 2) [Dataset]. *NASA National Snow and Ice Data Center Distributed Active Archive Center*. <https://doi.org/10.5067/D7GK8F5J8M8R>
- Rignot, E., Mougino, J., Scheuchl, B., van den Broeke, M., van Wessem, M. J., & Morlighem, M. (2019). Four decades of Antarctic Ice Sheet mass balance from 1979–2017. *Proceedings of the National Academy of Sciences of the United States of America*, *116*(4), 1095–1103. <https://doi.org/10.1073/pnas.1812883116>
- Robel, A. A., Wilson, E., & Seroussi, H. (2022). Layered seawater intrusion and melt under grounded ice. *The Cryosphere*, *16*(2), 451–469. <https://doi.org/10.5194/tc-16-451-2022>
- Sauthoff, W., & Freer, B. (2024). Subglacial water flow paths beneath Whillans Ice Plain, West Antarctica (Version 1.0) [Dataset]. *NERC EDS UK Polar Data Centre*. <https://doi.org/10.5285/0df5d4e9-2fcd-4420-b403-24d76848a5a5>
- Scambos, T. A., Berthier, E., & Shuman, C. A. (2011). The triggering of subglacial lake drainage during rapid glacier drawdown: Crane Glacier, Antarctic Peninsula. *Annals of Glaciology*, *52*(59), 74–82. <https://doi.org/10.3189/172756411799096204>
- Schmeltz, M., Rignot, E., & MacAyeal, D. R. (2001). Ephemeral grounding as a signal of ice-shelf change. *Journal of Glaciology*, *47*(156), 71–77. <https://doi.org/10.3189/172756501781832502>
- Schutz, B. E., Zwally, H. J., Shuman, C. A., Hancock, D., & DiMarzio, J. P. (2005). Overview of the ICESat Mission. *Geophysical Research Letters*, *32*(21), L21S01. <https://doi.org/10.1029/2005GL024009>



- Sergienko, O. V., & Haseloff, M. (2023). “Stable” and “unstable” are not useful descriptions of marine ice sheets in the Earth’s climate system. *Journal of Glaciology*, 69(277), 1483–1499. <https://doi.org/10.1017/jog.2023.40>
- Sergienko, O. V., MacAyeal, D. R., & Bindschadler, R. A. (2007). Causes of sudden, short-term changes in ice-stream surface elevation. *Geophysical Research Letters*, 34(22), L22503. <https://doi.org/10.1029/2007GL031775>
- Seroussi, H., Nowicki, S., Payne, A. J., Goelzer, H., Lipscomb, W. H., Abe-Ouchi, A., et al. (2020). ISMIP6 Antarctica: A multi-model ensemble of the Antarctic ice sheet evolution over the 21st century. *The Cryosphere*, 14(9), 3033–3070. <https://doi.org/10.5194/tc-14-3033-2020>
- Shepherd, A., Gilbert, L., Muir, A. S., Konrad, H., McMillan, M., Slater, T., et al. (2019). Trends in Antarctic Ice Sheet elevation and mass. *Geophysical Research Letters*, 46(14), 8174–8183. <https://doi.org/10.1029/2019GL082182>
- Shreve, R. L. (1972). Movement of water in glaciers. *Journal of Glaciology*, 11(62), 205–214. <https://doi.org/10.3189/S002214300002219X>
- Siegfried, M. R., & Fricker, H. A. (2018). Thirteen years of subglacial lake activity in Antarctica from multi-mission satellite altimetry. *Annals of Glaciology*, 59(76), 42–55. <https://doi.org/10.1017/aog.2017.36>
- Siegfried, M. R., & Fricker, H. A. (2021). Illuminating active subglacial lake processes with ICESat-2 laser altimetry. *Geophysical Research Letters*, 48(14), e2020GL091089. <https://doi.org/10.1029/2020GL091089>
- Siegfried, M. R., Fricker, H. A., Carter, S. P., & Tulaczyk, S. (2016). Episodic ice velocity fluctuations triggered by a subglacial flood in West Antarctica. *Geophysical Research Letters*, 43(6), 2640–2648. <https://doi.org/10.1002/2016GL067758>
- Siegfried, M. R., Venturelli, R. A., Patterson, M. O., Arnuk, W., Campbell, T. D., Gustafson, C. D., et al. (2023). The life and death of a subglacial lake in West Antarctica. *Geology*, 51(5), 434–438. <https://doi.org/10.1130/G50995.1>
- Simkins, L. M., Anderson, J. B., Greenwood, S. L., Gonnermann, H. M., Prothro, L. O., Halberstadt, A. R. W., et al. (2017). Anatomy of a meltwater drainage system beneath the ancestral East Antarctic ice sheet. *Nature Geoscience*, 10(9), 691–697. <https://doi.org/10.1038/ngeo3012>
- Slater, T., Shepherd, A., McMillan, M., Leeson, A., Gilbert, L., Muir, A., et al. (2021). Increased variability in Greenland Ice Sheet runoff from satellite observations. *Nature Communications*, 12(1), 6069. <https://doi.org/10.1038/s41467-021-26229-4>
- Smith, B., Adusumilli, S., Csathó, B. M., Felikson, D., Fricker, H. A., Gardner, A., et al. (2023). ATLAS/ICESat-2 L3A land ice height (version 6) [Dataset]. *NASA National Snow and Ice Data Center Distributed Active Archive Center*. <https://doi.org/10.5067/ATLAS/ATL06.006>
- Smith, B., Fricker, H. A., Gardner, A. S., Medley, B., Nilsson, J., Paolo, F. S., et al. (2020). Pervasive ice sheet mass loss reflects competing ocean and atmosphere processes. *Science*, 368(6496), 1239–1242. <https://doi.org/10.1126/science.aaz5845>
- Smith, B., Jelley, B. P., Dickinson, S., Sutterley, T., Neumann, T., & Harbeck, K. (2024). ATLAS/ICESat-2 L3B gridded Antarctic and Greenland height change (version 4) [Dataset]. *NASA National Snow and Ice Data Center Distributed Active Archive Center*. <https://doi.org/10.5067/ATLAS/ATL15.004>
- Stearns, L. A., Smith, B. E., & Hamilton, G. S. (2008). Increased flow speed on a large East Antarctic outlet glacier caused by subglacial floods. *Nature Geoscience*, 1(12), 827–831. <https://doi.org/10.1038/ngeo356>
- Stokes, C. R., & Clark, C. D. (2002). Ice stream shear margin moraines. *Earth Surface Processes and Landforms*, 27(5), 547–558. <https://doi.org/10.1002/esp.326>
- Stubblefield, A. G., Creyts, T. T., Kingslake, J., Siegfried, M. R., & Spiegelman, M. (2021). Surface expression and Apparent timing of Subglacial Lake Oscillations controlled by viscous ice flow. *Geophysical Research Letters*, 48(17), e2021GL094658. <https://doi.org/10.1029/2021GL094658>
- Stubblefield, A. G., Meyer, C. R., Siegfried, M. R., Sauthoff, W., & Spiegelman, M. (2023). Reconstructing subglacial lake activity with an altimetry-based inverse method. *Journal of Glaciology*, 1–15. <https://doi.org/10.1017/jog.2023.90>
- Sun, S., Pattyn, F., Simon, E. G., Albrecht, T., Cornford, S., Calov, R., et al. (2020). Antarctic ice sheet response to sudden and sustained ice-shelf collapse (ABUMIP). *Journal of Glaciology*, 66(260), 891–904. <https://doi.org/10.1017/jog.2020.67>
- Sun, X., Abshire, J. B., Borsa, A. A., Fricker, H. A., Yi, D., DiMarzio, J. P., et al. (2017). ICESat/GLAS altimetry measurements: Received signal dynamic range and saturation correction. *IEEE Transactions on Geoscience and Remote Sensing: A Publication of the IEEE Geoscience and Remote Sensing Society*, 55(10), 5440–5454. <https://doi.org/10.1109/TGRS.2017.2702126>
- Sutterley, T. C., Alley, K., Brunt, K., Howard, S., Padman, L., & Siegfried, M. (2017). pyTMD: Python-based tidal prediction software (Version 2.1.0) [Software]. *Zenodo*. <https://doi.org/10.5281/zenodo.5555395>
- Whiteford, A., Horgan, H. J., Leong, W. J., & Forbes, M. (2022). Melting and refreezing in an ice shelf basal channel at the grounding line of the Kamb Ice Stream, West Antarctica. *Journal of Geophysical Research: Earth Surface*, 127(11), e2021JF006532. <https://doi.org/10.1029/2021JF006532>
- Wiens, D. A., Aster, R. C., Nyblade, A. A., Bromirski, P. D., Gerstoft, P., & Stephen, R. A. (2024). Ross Ice Shelf displacement and elastic plate waves induced by Whillans Ice Stream slip events. *Geophysical Research Letters*, 51(7), e2023GL108040. <https://doi.org/10.1029/2023GL108040>
- Winberry, J. P., Anandakrishnan, S., Alley, R. B., Bindschadler, R. A., & King, M. A. (2009). Basal mechanics of ice streams: Insights from the stick-slip motion of Whillans Ice Stream, West Antarctica. *Journal of Geophysical Research*, 114(F1), F01016. <https://doi.org/10.1029/2008JF001035>
- Winberry, J. P., Anandakrishnan, S., Alley, R. B., Wiens, D. A., & Pratt, M. J. (2014). Tidal pacing, skipped slips and the slowdown of Whillans Ice Stream, Antarctica. *Journal of Glaciology*, 60(222), 795–807. <https://doi.org/10.3189/2014JG14J038>
- Zwally, H. J., Schutz, B., DiMarzio, J. P., & Hancock, D. (2014). GLAS/ICESat L1B Global elevation data (HDF5) (version 34) [Dataset]. *NASA National Snow and Ice Data Center Distributed Active Archive Center*. <https://doi.org/10.5067/ICESAT/GLAS/DATA109>